

**GRAVITY COMPENSATION OF A 2R1T
MECHANISM WITH REMOTE
CENTER OF MOTION FOR MINIMALLY
INVASIVE TRANSNASAL SURGERY
APPLICATIONS**

**A Thesis Submitted to the
Graduate School of Engineering and Sciences of
İzmir Institute of Technology
in Partial Fulfillment of the Requirements for the Degree of**

MASTER OF SCIENCE

in Mechanical Engineering

**by
Ataol Behram ALDANMAZ**

**September 2021
İZMİR**

ACKNOWLEDGEMENTS

First of all, I would like to sincerely thanks to my supervisor Assoc. Prof. Dr. Gökhan Kiper for his guidance throughout my academic life and his academic support for my thesis study. I also would like to thank to my co-supervisor Assoc. Prof. Dr. Mehmet İsmet Can Dede for his suggestions and ideas throughout my thesis study.

I would like to thank to my jury members, Prof. Dr. H. Seçil Artem for her great lectures through my bachelor and master degree classes, her suggestions for my thesis study and attending at my thesis defense seminar. I would also like to thank to Assist. Prof. Dr. Özgür Kilit for attending to my thesis defense seminar and his valuable recommendations.

I would like to thank to my family for their love and support through my life. They had supported me in all ways so I could improve myself in my field of interest. My dogs Bulut and Dalga have supported me with their lovely smiling faces when I came from my laboratory to home every evening and spread joy to my life. I wouldn't be able to complete this study without their support.

I would like to thank to Orhan Ayit which has helped me in multiple areas, came to help in the assembly section and gave suggestions to improve my study. He has been a valuable friend and co-worker.

I would also thank to Tarık Büyüköztekin for his practical solutions to my problems and help in the manufacturing of the parts. I would also like to thank to İbrahimcan Görgülü for his help in assembling of the system.

This study is funded by 1003 – Support Program for R&D Projects in Priority Areas of The Scientific and Technological Research Council of Turkey (TÜBİTAK) with the project name “Design of an Inherently Balanced Robotic Manipulator with Remote Center of Motion to be used as an Endoscope Holder for Endonasal Skull Base Surgery (BalanScope)” and the grant number 219M483

ABSTRACT

GRAVITY COMPENSATION OF A 2R1T MECHANISM WITH REMOTE CENTER OF MOTION FOR MINIMALLY INVASIVE TRANSNASAL SURGERY APPLICATIONS

In this work, gravity balancing of a 2URRR-URR parallel manipulator is issued. The manipulator is designed as an endoscope holder for minimally invasive transnasal pituitary gland surgery application. In the surgery, the endoscope is placed through the nostril of the patient where there is a natural path to the pituitary gland. In case of a motor failure, in order to protect the patient and to ease the control of the manipulator static balancing for this manipulator is worked out, the manipulator prototype is balanced and tested. The parallel manipulator has three legs. The payload mass has been distributed to side legs due to workspace limitations. By using counter-mass for two links in each leg, the center of mass of each leg has been reduced to the proximal link which simplified the balancing problem to balancing of a two degree-of-freedom inverted pendulum. By connecting a zero free length spring to the proximal link the total mass of the leg the manipulator has been kept in static balance in its desired workspace. Simulations show that with the applied design, torque effects on the motors have been reduced by 93.5%. Finally, the balancing solution is applied on the manipulator with active motors and the manipulator has been balanced, the torque values mostly has been decreased where the joint clearance, spring tension adjustments and mechanical constraints has affected the results. With the elimination of the joint clearance, mechanical constraints and rearranging the spring tension the required torque could be minimized.

ÖZET

MİNİMAL İNVAZİV TRANSNAZAL CERRAHİ UYGULAMALARI İÇİN UZAK HAREKET MERKEZLİ 2R1T MEKANİZMASININ YERÇEKİMİ DENGELENMESİ

Bu çalışmada 2URRR-URR paralel bir manipülatörün yerçekimi dengelenmesi çalışılmıştır. Manipülatör, minimal invaziv transnasal hipofiz bezi cerrahisi uygulaması için bir endoskop tutucu olarak tasarlanmıştır. Cerrahi operasyonda hastanın burun deliğinden hipofiz bezine giden doğal bir yoldan endoskop yerleştirilir ve operasyon gerçekleşir. Bu esnada motorlarda her hangi bir arıza olması halinde manipülatörün konumunu koruması ve manipülatörün kontrollünün kolaylaşması için bu çalışmada statik dengeleme çözümü geliştirilmiş, manipülatör prototipi dengelenmiş ve test edilmiştir. Paralel manipülatörün üç bacağı olup, manipülatörün çalışma alanı kısıtları nedeniyle uç-işlemci kütlesi iki bacağına dağıtılmıştır. Her bacakta üç uzuv olup ikisi karşıt kütle kullanılarak bacağın toplam kütlesi sabit platforma bağlı uzva indirgenerek dengeleme problemi iki serbestlik dereceli bir ters sarkacın dengelenme problemine dönüşmüştür. Sabit platforma bağlı uzvun üzerine yerleştirilen ek bir parçaya bir adet yayın bağlanmasıyla manipülatörün istenilen çalışma alanında statik dengelenmesi sağlanmış ve benzetim sonuçlarına göre motor torklarında dengelenmemiş haline göre 93.5% bir düşüş gözlemlenmiştir. Son olarak, dengeleme çözümü prototip üzerinde motorlar aktif durumda uygulanmıştır. Manipülatör dengelemeye ulaşılmış olsada sistemde bulunan boşluk, burulma ve yayların gerginlik ayarları nedeniyle motorların uygulaması gereken torklar çoğunlukla düşmüş olsa da bazı konumlarda bu durum değişmektedir. Sistemdeki boşluğun alınması, mekanik kısıtların giderilmesi ve yayların daha iyi bir şekilde gerilmesi ile daha iyi tork sonuçları alınabilir.

TABLE OF CONTENTS

ABSTRACT.....	iii
ÖZET	iv
LIST OF TABLES.....	vi
TABLE OF FIGURES.....	vii
CHAPTER 1 INTRODUCTION.....	1
CHAPTER 2 CALCULATIONS AND DESIGN	6
2.1 Distal Link Counter Mass Design	17
2.2 Middle Link Counter Mass Design	21
CHAPTER 3 TEST.....	31
3.1 Test #1: Spring Coefficient Test	31
3.2 Test #2: Individual Link – Counter-Mass Balancing Test	33
3.3 Test #3: Manipulator Assembled with Counter-Mass, Spring and Disabled Motors	37
3.4 Test #4: Parallel Manipulator Assembled with Counter-Mass, Spring and Running Motors.....	42
CHAPTER 4 CONCLUSION	51
REFERENCES	55

LIST OF TABLES

<u>Table</u>	<u>Page</u>
Table 1: Leg link lengths	12
Table 2: Maximum and minimum angles between proximal link and x-axis	15
Table 3: Maximum and minimum angles between proximal link and middle link	16
Table 4: Maximum and minimum angle between middle link and distal link	16
Table 5: Symbol definitions for D_CM_P3 and D_CM_P4.....	18
Table 6: Symbol definitions for CM_P3 and CM_P4	22
Table 7: Design specifications of balancing components.....	26
Table 8: Torque values on each actuator without balancing – dynamic analysis.....	27
Table 9: Torque values on each Actuator without balancing for static analysis	28
Table 10: Maximum - Minimum RMS total torque results (dynamic analysis) - N.m ..	30
Table 11: Position data from balanced manipulator with disabled motors.....	41
Table 12: Balanced manipulator with disabled motors workspace	41
Table 13: Counter mass Positions.....	44
Table 14: Balanced manipulator position data	46
Table 15: Balanced manipulator joint clearance.....	47
Table 16: Plane angles measured with FARO for the balanced manipulator	48
Table 17: Balanced manipulator torque results for each actuator.....	48
Table 18: Unbalanced manipulator position data	49
Table 19: Unbalanced manipulator torque results for each actuator	50

TABLE OF FIGURES

<u>Figure</u>	<u>Page</u>
Figure 1: Kinematic diagram of the 2URRR-URR parallel manipulator with remote center of motion D about which the platform has 2 rotations and 1 translation	4
Figure 2: Endonasal pituitary surgery	4
Figure 3: Diagram for the hybrid static force balancing of a leg with three links in series and with two counter masses and a spring	7
Figure 4: Kinematic diagram of the mechanism.	7
Figure 5: Simplified kinematic diagram with intersecting planes	8
Figure 6: Views normal to a) \vec{n}_3 or plane $\vec{x}_3\vec{z}_3$, b) $\vec{y}_3\vec{z}_3$ plane.	10
Figure 7: Balanced parallel manipulator	11
Figure 8: Payload mass calculation	12
Figure 9: Diagram for a basic gravity equilibrator using a zero-free length spring pulley	13
Figure 10: Passive arm and parallel manipulator assembly	14
Figure 11: (a) Maximum and (b) minimum angle between proximal link and x-axis.	15
Figure 12: (a) Maximum and (b) minimum angle between proximal link and middle link	16
Figure 13: Maximum and minimum angle between middle link and distal link	16
Figure 14: Distal link counter mass components mass calculations with respect to moment equilibrium	18
Figure 15: D_CM_P1 and D_CM_P2 assembly	18
Figure 16: D_CM_P2 and D_CM_P3 CoM	19
Figure 17: Middle link counter-mass components mass calculations with respect to moment equilibrium	21
Figure 18: CM_P3 and CM_P4 assembly	22
Figure 19: CM_P3 and CM_P4 CoM	23
Figure 20: General average RMS torque with respect to b_c and b_b for dynamic analysis.	29

<u>Figure</u>	<u>Page</u>
Figure 21: Spring coefficient calculation experiment setup, (a) close range, (b) distant view.....	31
Figure 22: Left leg spring force (N) vs elongation (mm) graph	32
Figure 23: Right leg spring force (N) vs elongation (mm) graph.....	32
Figure 24: Balanced left distal link.....	33
Figure 25: Balanced left distal link – 2.....	34
Figure 26: Balanced right distal link.....	34
Figure 27: Balanced right distal link – 2.....	35
Figure 28: Balanced left middle link	35
Figure 29: Balanced left middle link – 2	36
Figure 30: Balanced right middle link	36
Figure 31: Balanced right middle link – 2	37
Figure 32: Wire connection to proximal link.....	38
Figure 33: Wire tension adjustment.....	39
Figure 34: Balanced manipulator with motors disabled (a) front view, (b) side view ...	40
Figure 35: Balanced manipulator at (a) position #1 and (b) position #2	41
Figure 36: Balanced manipulator at (a) position #3 and (b) position #4	41
Figure 37: Balanced manipulator at (a) position #5 and (b) position #6	42
Figure 38: Bearing added on the pin.....	43
Figure 39: Cylindrical block position for middle and distal counter masses.....	44
Figure 40: Illustration of the leg for the parallel manipulator	47
Figure 41: Balanced manipulator torque results for each position	49
Figure 42: Unbalanced manipulator torque results for each position.....	50

CHAPTER 1

INTRODUCTION

A mechanism is statically balanced when its total potential energy is kept constant in any configuration of the mechanism. The mechanism which is in static equilibrium is constantly neutral equilibrium and its actuators are not required to sustain any conservative force acting on its moving members (Martini et al., 2015).

In most applications, the potential energy of a mechanism is due to gravitational potential and in this case static balancing corresponds to gravity balancing or gravity compensation. There are a few ways to obtain a gravity balanced system for parallel manipulators. If the overall center of mass (CoM) of the mechanism could be kept in the same level of height for any given configuration, the static balance is obtained in any direction in the space which is important because the unbalanced forces could cause vibrations, wear etc. (Jean and Gosselin, 1996). Another way to obtain a statically balanced mechanism is to keep its total energy constant so it could be statically balanced in the direction of the gravity vector (Russo et al., 2005)

To move a statically balanced system the redistribution of the potential energy within the system is important. A statically balanced system has many numbers of contribution to the mechanism. The effects of the undesired conservative forces are reduced by offsets to obtain a statically balanced system which improves the feedback with less error. The decrement in the operating effort of the actuators give opportunity for usage of smaller actuators with no or less amount of necessary energy to carry the weights. Statically balanced systems have a very good energy exchange between the energy storage elements and the system, so the mechanism does not need any operating force or energy. The only external energy would be needed to cover the energy losses due to friction etc. or to accelerate the mechanism (Herder, 2001)

Static balancers can be divided in to two areas. The first is with respect to the forces that had been balanced in the system like the weight, spring forces and other

conservative forces. The second one is with respect to the balancing principle which could be counterweight, springs, etc.

The type of static balancers that are issued in this work are with respect to the balancing principle, which will be the counter-weight and springs. Balancing with counterweight is a way that is preferred and used generally to balance the undesired weights. The main idea of using counterweight is to exchange the gravity potential between the counterweight and the balanced mass. One of the disadvantages of this balancing method is that it increases the inertia of the system and could cause collisions between the links in their workspace.

Spring to spring balancing or with another name spring force compensation is called when springs are balancing each other. In this type of balancing principle there is a special case is the redistribution of elastic tension in special construction elements (Herder, 2001). The disadvantage of spring-to-spring balancing is that it requires complex structures within the system which could limit the movement of the manipulator.

There are many of researches working on static balancing of parallel and serial manipulators for planar and spatial motion. Martini et al. (2019) worked on an algorithm for balancing serial and parallel mechanisms where counterweight, springs and combination of counterweights and springs are used together. For a given mechanism with a solvable forward kinematics and with the data about the balancing elements that would be used, the algorithm searches a convenient combination of the counterweight and springs without using any auxiliary links. The balancing parameters are determined by a numerical optimization procedure for maximizing the mechanism energy efficiency. The results are listed with respect to energy efficiency, instantaneous motor torque and joint reactions.

Wang and Kong (2019) developed a geometric method for static balancing of spherical mechanisms. The static balance is achieved by using a spring for each link without any auxiliary parallelograms.

Each moving link of the manipulator is balanced by fixing a spring between a point above the intersection of the joint axis and a point that is on a line defined by the intersection point and the equivalent CoM of the corresponding link.

Once a system is statically balanced by its balancers the system can operate in an energy free manner. Within the same system when the payload mass changes

compensation balancers should be adjusted. Van Dorsser et al. (2008) developed a system to adjust a spring and a linkage-based balancer by changing the active coils of the spring which effects its spring stiffness and allows the system to stay in balance when the payload changes in an energy conserving way. Kilit et al. (2015) have introduced a cam-spring model to statically balance a serial R mechanism with moment equilibrium, and showed that it is applicable to 2R serial mechanisms.

Maroof et al. (2021) have introduced a partial gravity compensation solution with springs and worked on the optimization of the balancing components for the 2URRR-URR parallel manipulator introduced by Yaşır et al. (2020). Partial gravity compensation has been achieved by enclosing a spiral spring within the actuation system where the springs are located on the rotating shafts. The optimization of the compact solution with torsional springs has been done by the partial swarm optimization (PSO). PSO has been used to arrange the spring stiffness value and preload initial angle for the actuators. As a result, they have found that it is possible to minimize the gravitational loads with the introduced design. Where the gravitational loads are not fully compensated a counter-mass-spring hybrid solution has been suggested.

In this work, gravity balancing of a 2URRR-URR parallel manipulator (Figure 1) is issued. The manipulator is designed as an endoscope holder for minimally invasive transnasal pituitary gland surgery application by Yaşır et al. (2020) and a balancing solution is previously proposed by Yaşır et al. (2019). In this work, this balancing solution is detailed, the manipulator prototype is balanced and tested.

In the aforementioned surgical operation, the manipulator is assembled on a passive serial robotic arm which is positioned by the surgeon. The end-effector of the parallel manipulator which is the endoscope is placed through the nostril of the patient where there is a natural path to the pituitary gland (Figure 2). By using additional surgical tools, the tumor is removed. Without any static balancing components on the system, the torques generated by the motors on the parallel manipulator would be high, make the system harder to control, consume more energy and also in case of a malfunction the manipulator would not be able to keep the position of the endoscope and would cause serious damage to the patient.

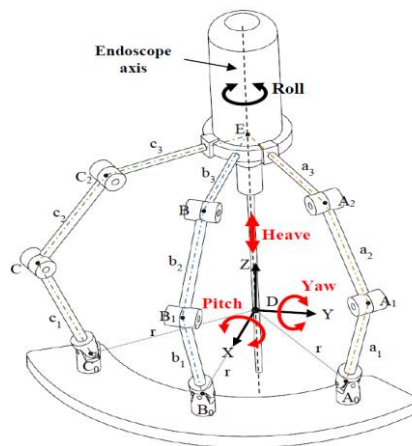


Figure 1: Kinematic diagram of the 2URR-URR parallel manipulator with remote center of motion D about which the platform has 2 rotations and 1 translation (Source: Yaşır, 2018).

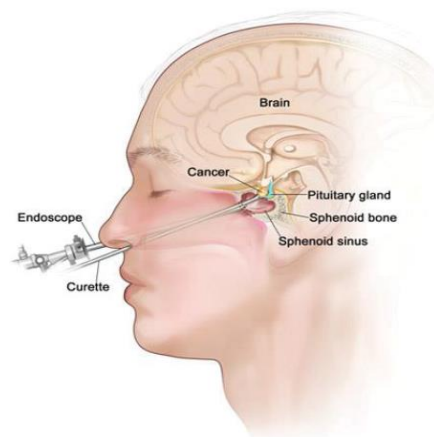


Figure 2: Endonasal pituitary surgery (Source: Best Spine & Neuro Care in India, 2018)

The requirements of the balancing system are that it should be as light-weighted as possible because the passive robotic arm end-effector has 10kg load limit and also in order not to increase the inertia. Also, the additional parts should not cause any link collisions. The parallel manipulator has a base and a moving platform which are connected to each other with three legs, each of which has three links. In order to avoid

link interferences, the middle leg is kept untouched and the payload mass is distributed to two of the legs. Using counter-weights,

CoM of distal links of each side leg are reduced to the proximal link attached to the base platform, so the balancing problem can be simplified to a basic gravity equilibrator (Herder, 2001), i.e., a spring balancer for an inverted pendulum.

For each leg, the spring is to be hidden behind a pulley or a pin to obtain an ideal zero free length spring, so that the tension in the wire is proportional to the length between the pulley and attachment point on the proximal link (Herder, 2001). The proximal link is connected to the base platform with a universal joint, so, line connecting the pin mounted on the base platform and the universal joint center should be along the gravity vector.

CHAPTER 2

CALCULATIONS AND DESIGN

Three static balancing solutions have been investigated: counter-mass balancing, spring balancing and the hybrid spring and counter-mass balancing.

When static balance is achieved with only adding counter-mass to the system, the increment in the weight is too high which is not a practical solution where the requirements for the study are to be lightweight and have a compact design. Extensions to the links on the legs cause collisions of the links among themselves, and with the other parts of the system and also with the patient.

Balancing using only springs causes a complicated design and too many numbers of springs added to the system. By introducing a hybrid solution, taking the reasonable parts of the two balancing principles (using counter-masses and springs) a more compact and lightweight design can be made as reported by Yaşır et al. (2019).

There are three links in each leg respect to the design specifications of the 2URRR-URR parallel manipulator (Figure 1. In Chapter 1). There are, one middle and two side legs. The center of mass (CoM) of each leg is represented as m_c , m_b and m_a in the order of distal link to proximal link. The mass of the payload is represented with m_{pay} which is the total mass of the platform group and including endoscope. M_c and M_b are the counter masses that has been used as the counter-mass balance part of the hybrid balancing solution.

The link lengths are represented as $r_c = |CG_p|$, $r_b = |AC|$, $r_a = |AA_0|$. The position of the counter masses is represented as $b_c = |CB_c|$ and $b_b = |AB_b|$. The positions of each link CoM are represented as $g_c = |CG_c|$, $g_b = |AG_b|$, $g_a = |A_0G_a|$ and the payload position is represented as $g_{\text{pay}} = r_c$ where the total leg CoM position is represented as $g_{a,t} = |A_0B_a|$. η is the angle between the proximal link and the x-axis, where gravity acts on $-y$ direction. $\eta_{\text{max}} = 89,63^\circ$ and $\eta_{\text{min}} = -64,11^\circ$. $\delta = 28.5^\circ$ is the assumed nominal angle between the base platform and horizontal level (x-axis) which could be seen from Figure 3.

respectively \vec{n}_1 , \vec{n}_2 and \vec{n}_3 . The fundamental rotation matrices about X-, Y- and Z-axes is denoted with $\hat{X}(\cdot)$, $\hat{Y}(\cdot)$ and $\hat{Z}(\cdot)$ respectively. Where all the planes include \vec{w} once θ_1 and θ_2 is defined the angle of the middle plane, θ_3 would be defined.

The angle of \vec{w} with respect to the XZ -plane is denoted with ϕ which corresponds to the pitch motion, the angle of \vec{w} with respect to the YZ-plane is denoted with ψ which corresponds to the yaw motion.

Unit normal vectors of left and side leg planes and along the end-effector axis could be calculated as follows,

$$\mathbf{n}_1 = [Z(\alpha_1)][Y(\beta)][X(\theta_1)] \begin{bmatrix} 0 \\ 1 \\ 0 \end{bmatrix} = \begin{bmatrix} c\alpha_1 s\beta s\theta_1 - s\alpha_1 c\theta_1 \\ s\alpha_1 s\beta s\theta_1 + c\alpha_1 c\theta_1 \\ c\beta s\theta_1 \end{bmatrix} \quad (2.1)$$

$$\mathbf{n}_2 = [Z(\alpha_2)][Y(\beta)][X(\theta_2)] \begin{bmatrix} 0 \\ 1 \\ 0 \end{bmatrix} = \begin{bmatrix} c\alpha_2 s\beta s\theta_2 - s\alpha_2 c\theta_2 \\ s\alpha_2 s\beta s\theta_2 + c\alpha_2 c\theta_2 \\ c\beta s\theta_2 \end{bmatrix} \quad (2.2)$$

Where $\mathbf{n}_1 \times \mathbf{n}_2$ is,

$$\mathbf{n}_1 \times \mathbf{n}_2 = \begin{bmatrix} (s\alpha_1 - s\alpha_2)c\beta s\beta s\theta_1 s\theta_2 + c\alpha_1 c\beta c\theta_1 s\theta_2 - c\alpha_2 c\beta s\theta_1 c\theta_2 \\ (c\alpha_2 - c\alpha_1)c\beta s\beta s\theta_1 s\theta_2 - s\alpha_2 c\beta s\theta_1 c\theta_2 + s\alpha_1 c\beta c\theta_1 s\theta_2 \\ s(\alpha_2 - \alpha_1)(c\theta_1 c\theta_2 + s^2\beta s\theta_1 s\theta_2) + c(\alpha_2 - \alpha_1)s\beta s(\theta_1 - \theta_2) \end{bmatrix} \quad (2.3)$$

Let $\alpha_1 = -\alpha$ and $\alpha_2 = \alpha$ then,

$$\mathbf{n}_1 \times \mathbf{n}_2 = \begin{bmatrix} -s\alpha s2\beta s\theta_1 s\theta_2 + c\alpha c\beta s(\theta_2 - \theta_1) \\ -s\alpha c\beta s(\theta_1 + \theta_2) \\ s2\alpha(c\theta_1 c\theta_2 + s^2\beta s\theta_1 s\theta_2) + c2\alpha s\beta s(\theta_1 - \theta_2) \end{bmatrix} \quad (2.4)$$

$$\Rightarrow |\mathbf{n}_1 \times \mathbf{n}_2| = \sqrt{(-s\alpha s2\beta s\theta_1 s\theta_2 + c\alpha c\beta s(\theta_2 - \theta_1))^2 + (s\alpha c\beta s(\theta_1 + \theta_2))^2 + (s2\alpha(c\theta_1 c\theta_2 + s^2\beta s\theta_1 s\theta_2) + c2\alpha s\beta s(\theta_1 - \theta_2))^2} \quad (2.5)$$

$$\mathbf{w} = \begin{bmatrix} s\psi \\ -s\phi \\ \sqrt{1-s^2\phi-s^2\psi} \end{bmatrix} = \frac{\mathbf{n}_1 \times \mathbf{n}_2}{|\mathbf{n}_1 \times \mathbf{n}_2|} \quad (2.6)$$

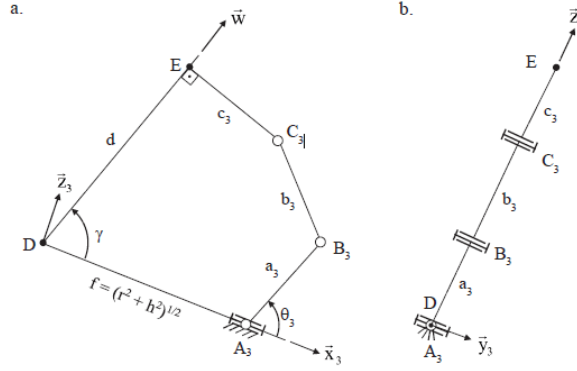


Figure 6: Views normal to a) \vec{n}_3 or plane $\vec{x}_3\vec{z}_3$, b) $\vec{y}_3\vec{z}_3$ plane

(Source: Yaşır 2019)

In Figure 6 end-effector line ED, platform group C_3E , middle leg $A_3B_3C_3$ and base group DA_3 are coplanar. Unit vector along DA_3 is denoted with \vec{x}_3 and its direction is obtained by rotating X-axis about Y-axis by angle β . Where $\vec{x}_3 = [c\beta \quad 0 \quad -s\beta]^T$ then $\widehat{A_3DE}$ angle could be found as,

$$A_3DE = \gamma = \cos^{-1}(\mathbf{w} \cdot \mathbf{x}_3) = \cos^{-1}(c\beta s\psi - s\beta\sqrt{1-s^2\phi-s^2\psi}) \quad (2.7)$$

Where \vec{x}_3 is the horizontal axis in the local coordinates' location of C_3 is $(d - ic_3)e^{i\gamma}$ and location of B_3 could be found as $f + a_3e^{i\theta_3}$ then,

$$|(d - ic_3)e^{i\gamma} - f - a_3e^{i\theta_3}| = b_3 \quad (2.8)$$

By doing forward kinematics by using equation 2.4 and 2.5 ψ and ϕ can be found from equation 2.9 and 2.10.

$$\psi = \sin^{-1} \frac{-s\alpha s 2\beta s\theta_1 s\theta_2 + c\alpha c\beta s(\theta_2 - \theta_1)}{|\mathbf{n}_1 \times \mathbf{n}_2|} \quad (2.9)$$

$$\phi = \sin^{-1} \frac{s\alpha c\beta s(\theta_1 + \theta_2)}{|\mathbf{n}_1 \times \mathbf{n}_2|} \quad (2.10)$$

To find d equation 2.8 is divided by $e^{i\gamma}$,

$$d = fc\gamma + a_3c(\theta_3 - \gamma) + \sqrt{b_3^2 - [c_3 - fs\gamma + a_3s(\theta_3 - \gamma)]^2} \quad (2.11)$$

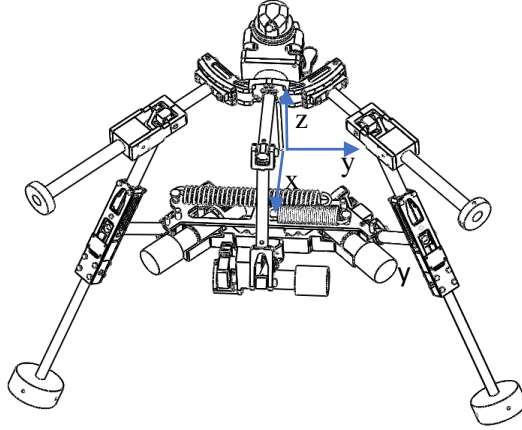


Figure 7: Balanced parallel manipulator

The workspace of the manipulator has been defined by Dede et al. (2018) by using accelerometers attached to the endoscope which is located in the nasal cavity and the data from the computed tomography scan. From the results it has been seen that the endoscope has 23° rotation range for pitch motion ($\Delta\phi$) and 33° rotation range for the yaw motion ($\Delta\psi$) about the pivot point and 95 mm for the heave motion along the pivot point for a transnasal operation. Due to safety conditions and considering that these values slightly change from patient to patient, the workspace of the manipulator has been selected as $\Delta\psi = 40^\circ$, $\Delta\phi = 30^\circ$ and $\Delta d = 100\text{mm}$. (Yaşır et. al. 2019)

Each leg has the same link length dimension parameters which are listed in Table 1.

Table 1: Leg link lengths

Leg Link Lengths (mm)				
r_c	r_b	r_a	b_c	b_b
200	195	135	115	220

The distances of the balancing masses to the corresponding joint axes, i.e. b_b and b_c , are selected by considering for minimum weight addition while avoiding link collisions. The masses of the links of side legs and middle leg are different with respect to their design properties. The counter masses for each leg structure has been calculated separately and has been tabulated in Table 7. The counter-mass values have been found by using moment equilibrium with respect to the corresponding joints. The formulization for the counter-masses and the distance of the CoM with respect to the origin which is located at joint A_0 is shown in Figure 3.

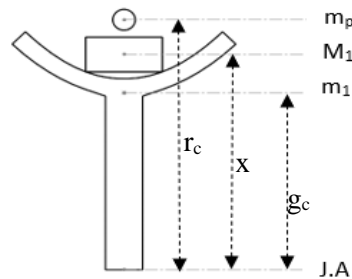


Figure 8: Payload mass calculation

To calculate the payload mass, moment equilibrium equations 2.12, 2.13 and 2.14 are written. Here, m_p is the calculated payload mass, M_1 is the endscope group mass and m_1 is the middle leg distal link mass (Figure 8) which also includes the platform and

the joint axis is where the distal link is connected to the middle link within the middle leg:

$$m_p r_c = M_l x + m_l g_c \Rightarrow m_p = \frac{M_l x + m_l g_c}{r_c} \quad (2.12)$$

$$M_c b_c = m_c g_c + m_{\text{pay}} r_c \Rightarrow M_c = \frac{m_c g_c + m_{\text{pay}} r_c}{b_c} \quad (2.13)$$

$$M_b b_b = m_b g_b + (M_c + m_c + m_{\text{pay}}) r_b \Rightarrow M_b = \frac{m_b g_b + (M_c + m_c + m_{\text{pay}}) r_b}{b_b} \quad (2.14)$$

The total leg mass, M_a , and the location of the CoM of the whole leg, $g_{a,t}$:

$$M_a = m_c + m_{\text{pay}} + m_b + m_a + M_c + M_b \quad (2.15)$$

$$M_a g_{a,t} = M_a r_a + m_a g_a \Rightarrow g_{a,t} = \frac{M_a r_a + m_a g_a}{M_a} \quad (2.16)$$

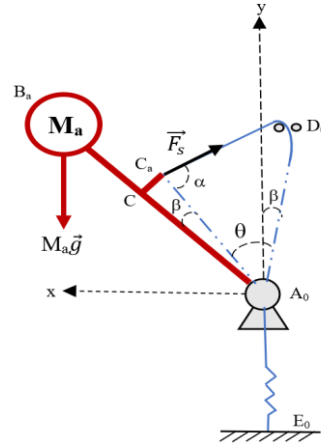


Figure 9: Diagram for a basic gravity equilibrator using a zero-free length spring pulley

The total mass of the leg M_a calculated from equation 2.15 is lumped at the CoM of the leg which is point B_a . When all the masses have been reduced to this point the

problem of balancing has been reduced to a basic gravity equilibrator problem as shown in Figure 8.

The angle β is introduced for ease of construction, but β has no effect on balancing calculations and it can be assumed as $\beta = 0$ (Herder, 2001).

$|A_0D_0| = f$, $|A_0C| = e$, where D_0 is a fixed point located on the string that is combined with a zero free length spring. To obtain an ideal zero-length spring the free length of the spring can be hidden behind a pulley or a pin. Using zero-length springs, the tension in the wire would be proportional to its length between the pulley and the connection point on the proximal link. By using the sine theorem in triangle A_0CD_0

$$\frac{f}{\sin \alpha} = \frac{|CD_0|}{\sin \theta} \Rightarrow |CD_0| = \frac{f \sin \theta}{\sin \alpha} \quad (2.17)$$

$s = |CD_0|$ is the effective spring displacement. Then the spring force F_s is

$$F_s = ks \quad (2.18)$$

Then by using equations 2.17, 2.18 and the moment equilibrium for M_a about A_0 , spring coefficient is found as:

$$g_{a,t} M_a g \sin \theta = e F_s \sin \alpha = e k s \sin \alpha = e f k \sin \theta \Rightarrow k = \frac{g_{a,t} M_a g}{e f} \quad (2.19)$$

The parallel manipulator is connected to an passive arm that positions the parallel manipulator, as can be seen from Figure 10.

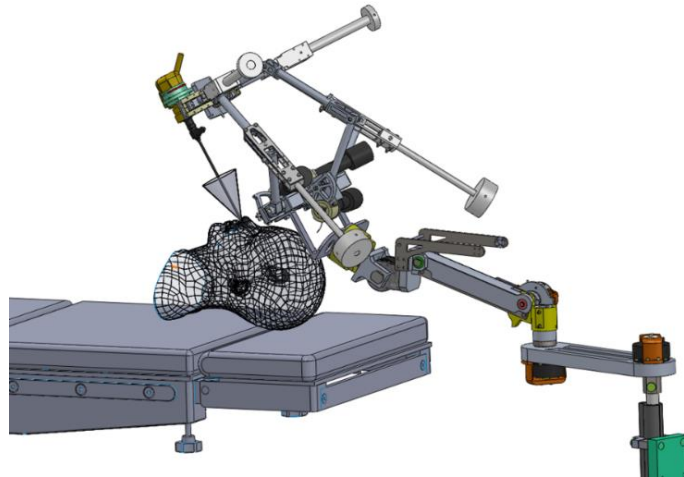


Figure 10: Passive arm and parallel manipulator assembly

When the middle leg is balanced due to the dimensions of the extension link for the middle link it collides with the passive arm. Because of this collision, the middle leg is not balanced. The payload is equally distributed to the left and right legs.

The counter-mass parts have been designed respect to the workspace of the manipulator. To avoid link collisions in each leg motion plane, middle leg motion has been analyzed. With the results, the angle range between each link has been calculated and been used as a design criterion for the counter-mass parts. The angle range between the links has been depicted in Figures 11-13 and Tables 2 where θ and γ show the angle between the links and between the endoscope and base group respectively.

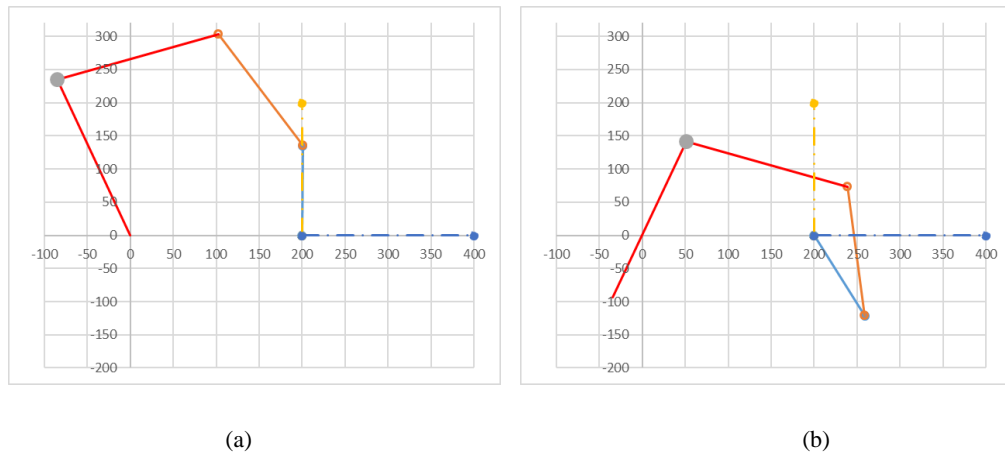


Figure 11: (a) Maximum and (b) minimum angle between proximal link and x-axis

Table 2: Maximum and minimum angles between proximal link and x-axis

Angle between proximal link and x-axis		
	max	min
θ_{px} (°)	89.63	-64.12
d (mm)	250	150
γ (°)	110	70

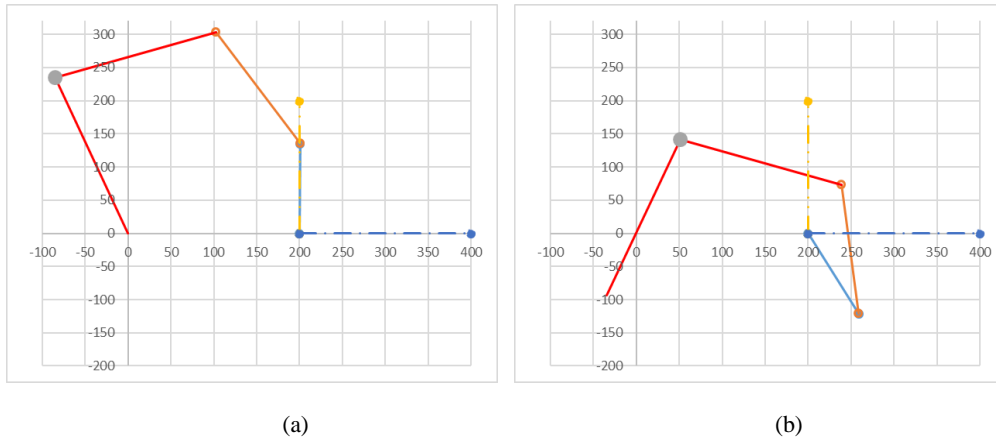


Figure 12: (a) Maximum and (b) minimum angle between proximal link and middle link

Table 3: Maximum and minimum angles between proximal link and middle link

Angle between proximal and middle link		
	max	min
θ_{pm} (°)	149.32	20.09
d (mm)	250	150
γ (°)	110	70

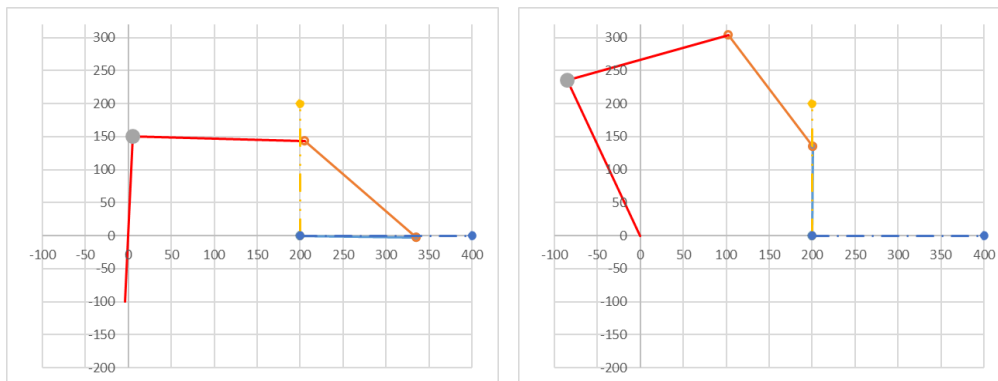


Figure 13: Maximum and minimum angle between middle link and distal link

Table 4: Maximum and minimum angle between middle link and distal link

Angle between middle and distal link		
	max	min
θ_{md} (°)	133.76	100.32
d (mm)	150	250
γ (°)	88	110

The counter mass parts have been designed to make as less changes as possible on the available link designs. These parts should have an adjustable part for the counter-mass and also meet the design criteria. To achieve these requirements counter-mass parts have been designed in two sections: one part that is adjustable and the other part to locate the adjustable part to the link. Two cylindrical parts are used for these two parts for ease of calculation. Where the connection elements mass and CoM are constant, to pull the center of mass of each link to the joint axis where the counter masses CoM are positioned at b_c and b_b , cylinder dimensions has been calculated.

2.1 Distal Link Counter Mass Design

M_c is the counter mass to balance the distal link. M_c consists of four parts named as D_CM_P1, D_CM_P2, D_CM_P3, D_CM_P4. The parts D_CM_P1 and D_CM_P2 are the connection elements where their mass and CoM positions with respect to the common joint axis are constant. The adjustable parts with M_c mass value lumped at the b_c distance are D_CM_P3 and D_CM_P4 which both are cylindrical parts.

The aim is to find the proper height and radius for these cylindrical parts so that the distal link would stay in static balance. Because of where D_CM_P3 connects with D_CM_P2, the radius of D_CM_P3 is already known. The unknowns are the radius and height of part D_CM_P4 and the height of D_CM_P3.

From Figure 14 the moment equilibrium equation 2.20 is written:

$$M_c b_c = m_c g_c + m_{\text{pay}} r_c \quad \Rightarrow \quad M_c = \frac{m_c g_c + m_{\text{pay}} r_c}{b_c} \quad (2.20)$$

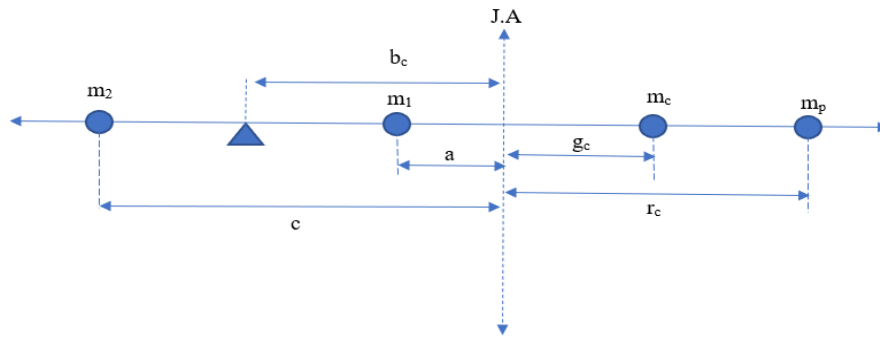


Figure 14: Distal link counter mass components mass calculations with respect to moment equilibrium

m_2 : The mass sum of D_CM_P3 and D_CM_P4, m_1 : The mass sum of two parts of D_CM_P1 and one D_CM_P2 and $M_c = m_2 + m_1$. By using the equality for M_c and leaving m_2 alone:

$$m_2 = M_c - m_1 = \frac{m_c g_c + m_{pay} r_c}{b_c} - m_1 \quad (2.21)$$

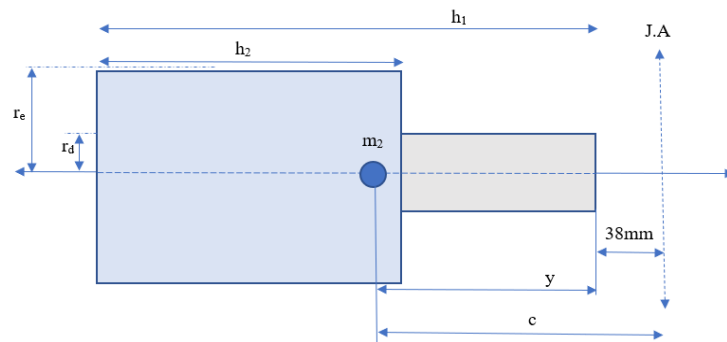


Figure 15: D_CM_P1 and D_CM_P2 assembly

Table 5: Symbol definitions for D_CM_P3 and D_CM_P4

Symbol	Definition
m_d	mass of D_CM_P3
h_1	height of D_CM_P3
r_d	radius of D_CM_P3
d_1	density of D_CM_P3
m_e	mass of D_CM_P4
h_2	height of D_CM_P4
r_e	radius of D_CM_P4
d_2	density of D_CM_P4

When D_CM_P3 is assembled with D_CM_P2 the base of the cylinder D_CM_P3 has a fixed distance to the joint axis which is 38 mm which is shown in Figure 15. Where “y” is the distance of the CoM of m_2 with respect to the base of D_CM_P3 shown in Figure 15 and d is the density of parts D_CM_P2, D_CM_P3 and D_CM_P3

- $V_d = \pi r_d^2 h_1 \Rightarrow m_d = d_1 \pi r_d^2 h_1$
- $V_e = \pi h_2 (r_e^2 - r_d^2) \Rightarrow m_e = d_2 \pi h_2 (r_e^2 - r_d^2)$

$$d_1 \pi r_d^2 h_1 + d_2 \pi h_2 (r_e^2 - r_d^2) = \frac{m_c g_c + m_p r_c}{b_c} - m_1 \quad (2.22)$$

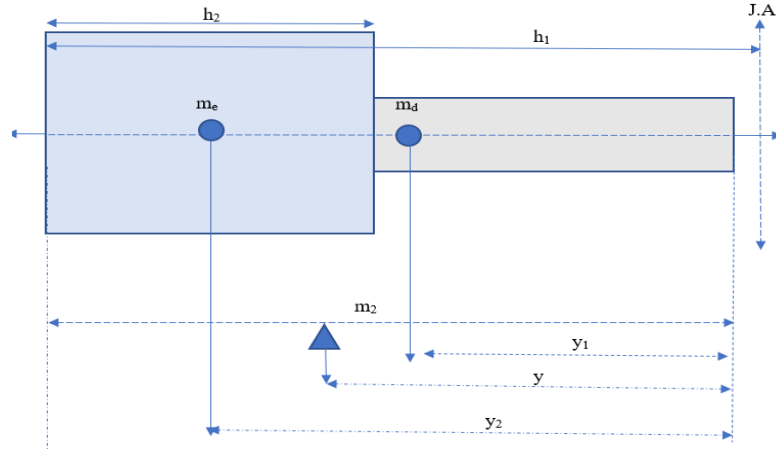


Figure 16: D_CM_P2 and D_CM_P3 CoM

By writing a moment equilibrium for m_d and m_e shown in Figure 16

$$(m_d + m_e) y = m_e y_2 + m_d y_1$$

$$y = \frac{m_e y_2 + m_d y_1}{m_d + m_e} \quad (2.23)$$

From Figure 14 moment equilibrium equation between the masses has been written:

$$m_2 c + m_1 a = m_c g_c + m_p r_c \Rightarrow c = \frac{m_c g_c + m_p r_c - m_1 a}{m_2} = \frac{m_c g_c + m_p r_c - m_1 a}{m_d + m_e} \quad (2.24)$$

where, $c = y + 38$ mm. By using Equation 2.23 and the relation $c = y + 38$ mm

$$\frac{m_c g_c + m_p r_c - m_1 a}{m_d + m_e} - 38 = \frac{m_e y_2 + m_d y_1}{m_d + m_e} \quad (2.25)$$

By implementing $y_2 = h_1 - \frac{h_2}{2}$ and $y_1 = \frac{h_1}{2}$ into Equation 2.25 where the center of mass of each cylinder is at the center of each cylinder:

$$m_e \left(h_1 - \frac{h_2}{2} + 38 \right) + m_d \left(\frac{h_1}{2} + 38 \right) = m_c g_c + m_p r_c - m_1 a \quad (2.26)$$

where $m_e = d_2 \pi h_2 (r_e^2 - r_d^2)$ and $m_d = d_1 \pi r_d^2 h_1$:

$$\begin{aligned} -h_2^2 \frac{d_2 \pi (r_e^2 - r_d^2)}{2} + h_2 d_2 \pi (r_e^2 - r_d^2) (h_1 + 38) + h_1^2 \frac{d_1 \pi r_d^2}{2} + h_1 d_1 \pi r_d^2 38 \\ = \\ m_c g_c + m_p r_c - m_1 a \end{aligned} \quad (2.27)$$

By rearranging Equation 2.22 by leaving h_2 alone;

$$h_2 = \frac{\left(\frac{m_c g_c + m_p r_c}{b_c} - m_1 \right) - d_1 \pi r_d^2 h_1}{d_2 \pi (r_e^2 - r_d^2)} = \frac{A - B h_1}{E} \quad (2.28)$$

where $A = \frac{m_c g_c + m_p r_c}{b_c} - m_1$, $B = d_1 \pi r_d^2$ and $E = d_2 \pi (r_e^2 - r_d^2)$.

To find h_1 , Equation 2.28 should be inserted into Equation 2.27 and also dimension for “ r_e ” should be given:

$$h_1^2 \left(\frac{-B}{2} - \frac{B^2}{2E} \right) + h_1 \left(\frac{AB}{E} + A \right) - \frac{A^2}{2E} + 38A - U = 0 \quad (2.29)$$

$$N h_1^2 + M h_1 + D = 0$$

- $N = -\frac{r_d^4 d_1^2 \pi^2}{2E} - \frac{r_d^2 d_1 \pi}{2}$
- $M = \frac{A r_d^2 d_1 \pi}{E} + A$
- $U = m_c g_c + m_p r_c - m_1 a$
- $D = \frac{-A^2}{2E} + 38A - U$

$$h_1 = \frac{-M \pm \sqrt{M^2 - 4ND}}{2N} \quad (2.30)$$

Once h_1 is found, h_2 could be found from Equation 2.28.

2.2 Middle Link Counter Mass Design

M_b is the counter mass value to balance the distal link. M_b consists of five parts named as CM_P1, CM_P1.2, D_CM_P2, CM_P3 and CM_P4. The parts CM_P1, CM_P1.2 and CM_P2 are the connection elements where their mass and CoM position with respect to the common joint axis are constant. The adjustable parts with mass M_b lumped at distance b_b are CM_P3 and CM_P4 which both are cylindrical parts.

The aim is to find the proper height and radius for these cylinders so that the middle link would remain in static balance. Because of where CM_P3 connects with CM_P2, the radius of CM_P3 is already known. The unknowns are the radius and height of part CM_P4 and the height of CM_P3.

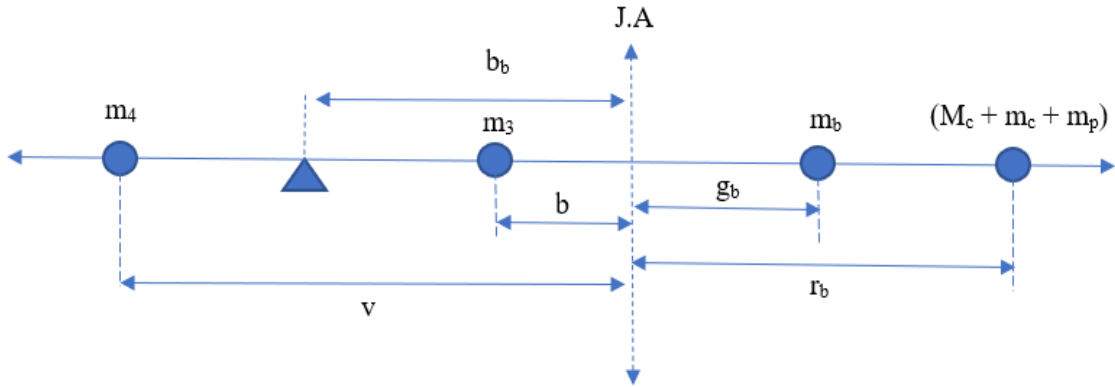


Figure 17: Middle link counter-mass components mass calculations with respect to moment equilibrium

$$M_b b_b = m_b g_b + (M_c + m_c + m_{pay}) r_b \Rightarrow M_b = \frac{m_b g_b + (M_c + m_c + m_{pay}) r_b}{b_b} \quad (2.31)$$

Where m_4 is the total mass of CM_P3, CM_P4, m_3 is the total mass of three parts of CM_P1, CM_P1.2 and CM_P2 and $M_b = m_3 + m_4$. By using the equality for M_b and leaving m_4 alone:

$$m_4 = M_b - m_3 = \frac{m_b g_b + (M_c + m_c + m_p) r_b}{b_b} - m_3 \quad (2.32)$$

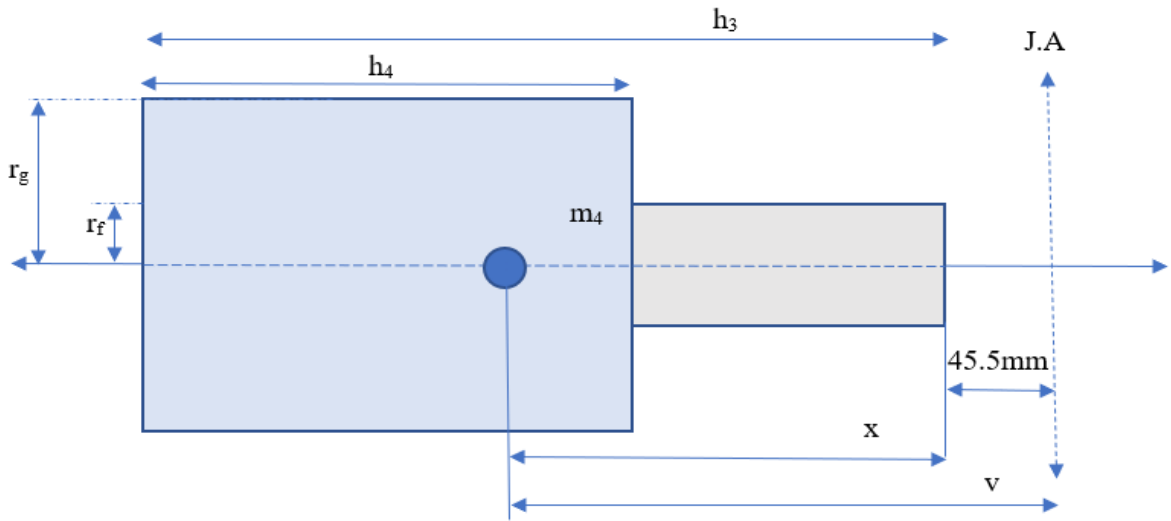


Figure 18: CM_P3 and CM_P4 assembly

Table 6: Symbol definitions for CM_P3 and CM_P4

Symbol	Definition
m_f	mass of CM_P3
h_3	height of CM_P3
r_f	radius of CM_P3
d_3	density of CM_P3
m_g	mass of CM_P4
h_4	height of CM_P4
r_g	radius of CM_P4
d_4	density of CM_P4

When CM_P3 is assembled with CM_P2 the base of the cylinder CM_P3 has a fixed distance to the joint axis which is 45.5 mm which is shown in Figure 18. x is the distance of the CoM of m_4 with respect to the base of CM_P3_V3 shown in Figure 18 and “ d ” is the density of parts CM_P2, CM_P3 and CM_P3.

$$V_f = \pi r_f^2 h_3 \Rightarrow m_f = d_3 \pi r_f^2 h_3$$

$$V_g = \pi h_4 (r_g^2 - r_f^2) \Rightarrow m_g = d_4 \pi h_4 (r_g^2 - r_f^2) \quad (2.33)$$

$$m_f + m_g = m_4 = M_b - m_3$$

$$d_3 \pi r_f^2 h_3 + d_4 \pi h_4 (r_g^2 - r_f^2) = \frac{m_b g_b + (M_c + m_c + m_p) r_b}{b_b} - m_3 \quad (2.34)$$

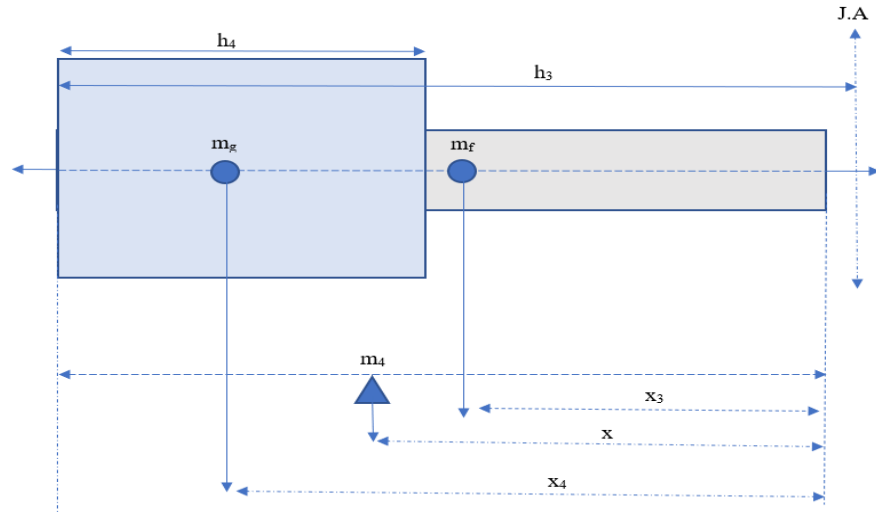


Figure 19: CM_P3 and CM_P4 CoM

From Figure 19,

$$(m_f + m_g)x = m_f x_3 + m_g x_4 \Rightarrow x = \frac{m_f x_3 + m_g x_4}{m_f + m_g} \quad (2.35)$$

From Figure 18,

$$m_4 v + m_3 b = m_b g_b + (M_c + m_c + m_p) r_b$$

$$v = \frac{m_b g_b + (M_c + m_c + m_p) r_b - m_3 b}{m_4} \quad (2.36)$$

where $v = x + 45.5 \text{ mm}$, $x_3 = \frac{h_3}{2}$, $x_4 = h_3 - \frac{h_4}{2}$, $m_4 = m_f + m_g$, $m_f = d_3 \pi r_f^2 h_3$ and $m_g = d_4 \pi h_4 (r_g^2 - r_f^2)$. By using Equation 2.35 and the relation $v = x + 45.5 \text{ mm}$,

$$\begin{aligned}
\frac{m_b g_b + (M_c + m_c + m_p)r_b - m_3 b}{m_4} &= \frac{m_f x_3 + m_g x_4}{m_f + m_g} + 45.5 \\
-h_4^2 \frac{d_4 \pi (r_g^2 - r_f^2)}{2} + h_4 d_4 \pi (r_g^2 - r_f^2) (h_3 + 45.5) + h_3^2 \frac{d_3 \pi r_f^2}{2} + 45.5 h_3 d_3 \pi r_f^2 & \\
= & \\
m_b g_b + (M_c + m_c + m_p)r_b - m_3 b &
\end{aligned} \tag{2.37}$$

By rearranging Equation 2.34 and leaving h_4 alone,

$$h_4 = \frac{\left(\frac{m_b g_b + (M_c + m_c + m_p)r_b}{b_b} - m_3\right) - d_3 \pi r_f^2 h_3}{d_4 \pi (r_g^2 - r_f^2)} = \frac{H - G h_3}{Q} \tag{2.38}$$

where $h = \left(\frac{m_b g_b + (M_c + m_c + m_p)r_b}{b_b} - m_3\right)$, $Q = d_4 \pi (r_g^2 - r_f^2)$ and $G = d_3 \pi r_f^2$.

To find h_3 , Equation 2.38 should be inserted into Equation 2.37 and also dimension for r_g should be given:

$$h_3^2 \left(-\frac{G}{2} - \frac{G^2}{2Q}\right) + h_3 \left(\frac{HG}{Q} + H\right) - \frac{H^2}{2Q} + 45.5H - m_b g_b - M = 0 \tag{2.39}$$

$$J h_3^2 + K h_3 + L = 0$$

- $J = -\frac{G}{2} - \frac{G^2}{2Q}$
- $K = \frac{HG}{Q} + H$
- $M = m_b g_b + (M_c + m_c + m_p)r_b - m_3 b$
- $L = -\frac{H^2}{2Q} + 45.5H - m_b g_b - M$

$$h_{3,1,2} = \frac{-K \pm \sqrt{K^2 - 4JL}}{2J} \tag{2.40}$$

Using the calculated values for h_3 , h_4 could be found from Equation 2.38. These calculations are repeated for each b_b and b_c value. b_b is in a range of [50, 300] and b_c is in a range of [100,300]. To find the best solution two necessary conditions has been determined:

Condition 1:

1. Height of $D_CM_P2_V3 + h_2 < h_1 \leq 270$ mm
2. $r_e/2 < h_2 \leq 80$ mm

Condition 2:

1. Height of $D_CM_P2_V3 + h_4 < h_3 \leq 250$ mm
2. $r_e/2 < h_2 \leq 80$ mm

From the results of this analysis, for dimension r_g , it has been found that when it decreases from its maximum value, 35 mm, by 5 mm and where r_e is kept constant the lengths of h_3 and h_4 increase. In this 5 mm range the smallest values for h_3 and h_4 are when r_g is equal to 35 mm and the total counter mass does not change. If this range has been increased from 5 mm to 10 mm, then after 5 mm until 10 mm decrement the total counter-mass increases where the dimensions for h_3 and h_4 are smaller than where r_g is equal to 35 mm.

The total counter-mass should be minimized as much as possible where the heights of h_3 and h_4 should be selected to prevent link collision. So, from the results r_g has been selected as 35 mm because of when r_g is equal to 35 mm, counter-mass is minimum and h_3 and h_4 does not cause any link collisions.

For r_e its minimum applicable dimension is 12 mm and until 24 mm its effect on the total counter-mass is zero. In this range h_1 and h_2 increase when r_e decreases. When r_e equals to 24 mm, the total counter-mass exceeds its lowest value and the minimum values for h_1 and h_2 (where the lowest counter-mass mass is achieved) is reached. So, r_e has been selected as 24 mm.

With selected values of $r_e = 24$ mm and $r_g = 35$ mm, $r_d = 8.5$ mm and $r_f = 6$ mm the design specifications have been listed in Table 7.

Table 7: Design specifications of balancing components

LEFT LEG	m_c (gr)	111.3	g_c (mm)	75.90938	h₁ (mm)	192.4055	b_c (mm)	115	M_c (gr)	843.5869	k (N/mm)	1.8041
	m_b (gr)	115.8	g_b (mm)	118.2294	h₂ (mm)	12.09209	b_b (mm)	220	M_b (gr)	1301.107	f (mm)	80.22409
	m_a (gr)	73.3	g_a (mm)	75.66227	h₃ (mm)	244.0932	g_{a,t} (mm)	133.4939	M_a (gr)	2887.913	e_L (mm)	26.13059
	m_p (gr)	442.8189	g_p (mm)	200	h₄ (mm)	29.70822						
RIGHT LEG	m_c (gr)	112.1	g_c (mm)	75.92179	h₁ (mm)	192.64	b_c (mm)	115	M_c (gr)	844.1271	k (N/mm)	1.5919
	m_b (gr)	116.1	g_b (mm)	118.2503	h₂ (mm)	12.06032	b_b (mm)	220	M_b (gr)	1302.467	f (mm)	80.22409
	m_a (gr)	74.4	g_a (mm)	77.68955	h₃ (mm)	244.0003	g_{a,t} (mm)	133.5256	M_a (gr)	2892.013	e_R (mm)	29.66288
	m_p (gr)	442.8189	g_p (mm)	200	h₄ (mm)	29.68952						

To reach proper results the mechanism has been simulated in Simulink which gives ability to simulate the torque effects of these extension link lengths on the actuators. By using MATLAB r2019b the codes to calculate the desired counter-mass values and spring constants has been written. To simulate the effects of the changes in the system to the torque on the motors Simulink/MATLAB r2019b has been used with the first-generation library.

The step time and ODE used in the simulation are 0.001 sec and Euler, respectively. The system has been simulated dynamically and statically to make a more correct comparison.

For ideal conditions when a mechanism is statically balanced, there should not be any torque effecting the actuators, where the actuators should only spend energy to accelerate or decelerate the mechanism.

For the mechanism that has been worked on, without any extra balancing members on the mechanism the torque values for each actuator have been calculated. To observe the mechanism within the end-effector workspace, a dynamic analysis has been carried out. For the dynamic motion testing an input trajectory is generated according to the data taken from the medical doctors.

When SimMechanics is analyzing the dynamic motion, the manipulator is tracing the workspace that has been determined by the ψ , ϕ angles and the d distance. While all of the area covered by the ψ ($\Delta\psi = 30^\circ$ around x – axis, Figure 7) and ϕ ($\Delta\phi = 40^\circ$ around y -axis, Figure 7) angles are traced, the d distance is analyzed in three steps. The heave motion is between a range of 150 mm and 250 mm. The heave motion is analyzed for d changing between 140 mm -150 mm, 195 mm - 205 mm and 240 mm - 250 mm. In

SimMechanics all variables are changed at the same time during the dynamic motion simulation to obtain a more comprehensive data about the manipulator.

To compare the balanced torque values firstly the torque values for each manipulator has been calculated where d is 155 mm, 200 mm and 245 mm as given Table 8. In these analyses to calculate the average RMS values coming from the three actuators Equation 2.30 has been used.

$$\sqrt{\frac{(RMS_1)^2+(RMS_2)^2+(RMS_3)^2}{3}} \quad (2.30)$$

where RMS_1: The RMS torque value for the left leg actuator, RMS_2: The RMS torque value for the right leg actuator and RMS_3: The RMS torque value for the middle leg actuator.

Table 8: Torque values on each actuator without balancing – dynamic analysis

d=245 mm, f=80.23 mm, e_L = 26.13 mm, e_R = 29.66 mm - Dynamic Analysis			
RMS_Left Actuator	RMS_Right Actuator	RMS_Middle Actuator	AVG RMS Torque
3.71 N·m	3.68 N·m	1.97 N·m	3.22 N·m
d=200 mm, f=80.23 mm, e_L = 26.13 mm, e_R = 29.66 mm - Dynamic Analysis			
RMS_Left Actuator	RMS_Right Actuator	RMS_Middle Actuator	AVG RMS Torque
3.58 N·m	3.55 N·m	2.11 N·m	3.15 N·m
d=155 mm, f=80.23 mm, e_L = 26.13 mm, e_R = 29.66 mm - Dynamic Analysis			
RMS_Left Actuator	RMS_Right Actuator	RMS_Middle Actuator	AVG RMS Torque
3.23 N·m	3.2 N·m	1.94 N·m	2.85 N·m
General AVG RMS Torque without Balance			
(Dynamic Analysis)			
3.08 N·m			
e : Position of acting spring force on proximal link with respect to A ₀ (Figure 6)			
e_L: Left Leg "e" value , e_R: Right Leg "e" value			

To obtain a more compact average RMS torque value which could be used as a general value for all positions of the manipulator the average of the average RMS torque values when d is equal to 155 mm, 200 mm and 245 mm has been taken by using Equation 14 and the general average RMS torque value without balancing is 3.08 N.m

For the balanced model, there are two extension link lengths $b_c = |CB_c|$ which is for the distal link balance and $b_b = |AB_b|$ (Figure 3) for the middle link balance.

During the analysis these b_c and b_b extension link lengths are taken to be equal variable for the right leg and left leg. To see the best solution b_c vary from 100 mm to 300 mm and b_b vary from 50 mm to 300 mm and the combination of all the possibilities has been investigated. Each extension link length has been increased 5 mm for each step and the analysis is completed with 2091 steps.

Firstly, the static analysis had been performed to see the torque values on the actuators for each situation of the extension link lengths. When there are no balancing elements on the manipulator and when d has values of 250 mm, 200 mm and 150 mm and $\delta = 28.5^\circ$ for the static analysis the torque values on the actuators are shown in Table 9.

Table 9: Torque values on each Actuator without balancing for static analysis

d=250 mm, f=80.23 mm, e_L = 26.13 mm, e_R = 29.66 mm - Static Analysis				
	RMS_Left Actuator	RMS_Right Actuator	RMS_Middle Actuator	AVG RMS Torque
	3.71 N·m	3.68 N·m	1.93 N·m	3.22 N·m
d=200 mm, f=80.23, e_L = 26.13 mm, e_R = 29.66 mm - Static Analysis				
	RMS_Left Actuator	RMS_Right Actuator	RMS_Middle Actuator	AVG RMS Torque
	3.57 N·m	3.55 N·m	2.11 N·m	3.15 N·m
d=150 mm, f=80.23 mm, e_L = 26.13 mm, e_R = 29.66 mm - Static Analysis				
	RMS_Left Actuator	RMS_Right Actuator	RMS_Middle Actuator	AVG RMS Torque
	3.18 N·m	3.15 N·m	1.9 N·m	2.81 N·m
General AVG RMS Torque without Balance				
(Static Analysis)				
3.06 N·m				
e : Position of acting spring force on proximal link with respect to A ₀ (Figure 6)				
e_L: Left Leg "e" value , e_R: Right Leg "e" value				

The RMS torque value with balancing is 0.106 N·m (constant) for varying b_c and b_b extension link lengths for the static analysis. The torque value is not zero, because the actuators' CoM positions are not exactly at the universal joint center A₀ (Figure 3) and generates a torque and the middle leg is not balanced because there is not enough space

for extension link b_b at the middle leg. There is a %93.5 decrease with respect to the general average RMS torque without balance.

To obtain more proper results that would be valid for the workspace of the manipulator, dynamic analysis had been carried out. From the dynamic analysis results it could be seen that for the minimum values of b_c and b_b the general average RMS torque value has decreased from 3.08 N·m to 0.20 N·m which is an %93.5 decrease. For the maximum values of b_c and b_b which are both 300 mm, the general average RMS torque value has been decreased to 0.204 N.m which corresponds to an %93.35 decrease. The general average RMS torque results for the dynamic analysis could be seen from Figure 20. The results show that the general average RMS torque slightly increases for larger values of the extension link lengths b_c and b_b .

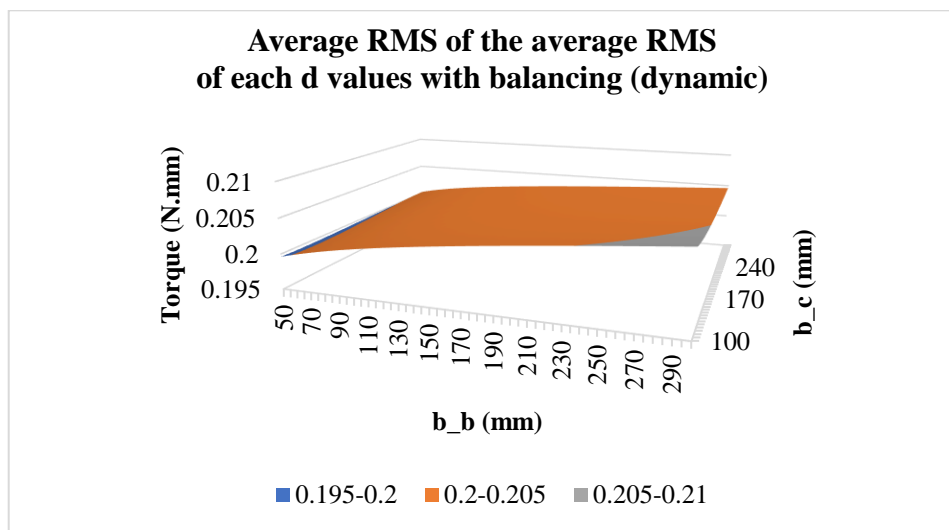


Figure 20: General average RMS torque with respect to b_c and b_b for dynamic analysis

The data from the dynamic analysis is divided where d is in the range of 140 mm-150 mm, 195 mm-205 mm and 240 mm-250 mm. The maximum, minimum values of the left, right, middle actuators and the average RMS torque values of these results for each range of d could be seen in Table 10.

Table 10: Maximum - Minimum RMS total torque results (dynamic analysis) - N.m

RMS Total Torque Results (Dynamic Analysis) N.m		
d=245 mm	d=200 mm	d=155 mm
max	max	max
0.187 N·m	0.209 N·m	0.222 N·m
min	min	min
0.183 N·m	0.202 N·m	0.213 N·m

From Table 10, it can be seen that as the d values increases the torque values on the actuators decrease. The minimum torque values are obtained where d is at its maximum which is the position where the tip of the endoscope is positioned at the entry of the nostril, the torque values start to slightly increase. When the tip of the endoscope reaches the surgery area where d = 150 mm the torque values on the actuator's peaks to its maximum value.

CHAPTER 3

TESTS

In this study four different set of tests have been performed: tests to determine the spring coefficients, balancing tests for the links with a counter-mass, balancing tests for the assembled manipulator with disabled motors and the final tests for the manipulator with functional motors.

3.1 Test #1: Spring Coefficient Test

The springs are manufactured in the industrial zone according to the design specifications calculated in Chapter 2. Ideally, the spring stiffness value should be 1.683 N/mm, but it is expected that the manufactured springs have different stiffness values. In order to determine the stiffness of the manufactured springs, a simple test setup has been built using a hinge, several weights and a ruler which could be seen in Figure 21.

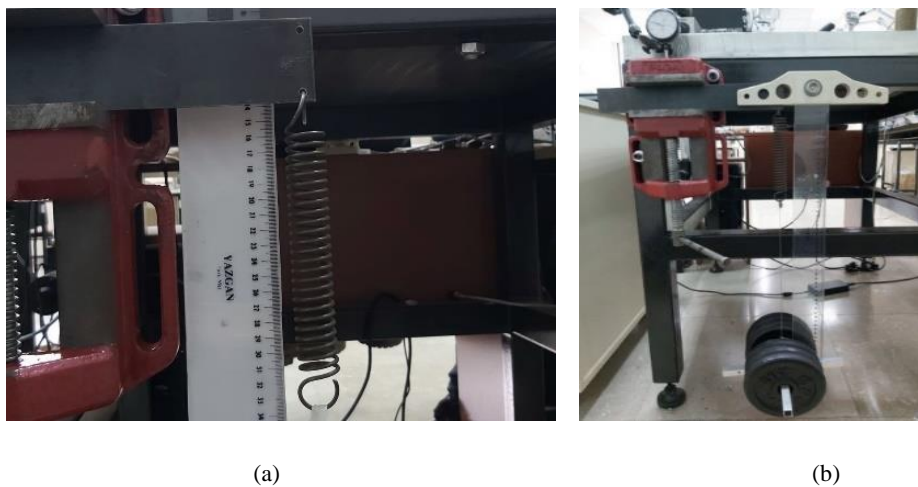


Figure 21: Spring coefficient calculation experiment setup, (a) close range, (b) distant view

First the free length of the spring has been measured with a caliper rule. Fixing one end of the spring and adding weight to the other end, the elongation of the spring has been recorded using the ruler. The weight that has been added to the free end of the spring has been changed and also each measurement has been made twice to see repeatability. From the data collected that could be seen in Figure 22-23 an approximately linear behavior has been observed. Fitting a linear line to each data, the spring coefficient and initial tension for each spring is determined. The stiffness values are determined as 1.8041 N/mm for the spring to be attached to the left leg, and 1.5919 N/mm for the spring to be attached to the right leg of the manipulator.

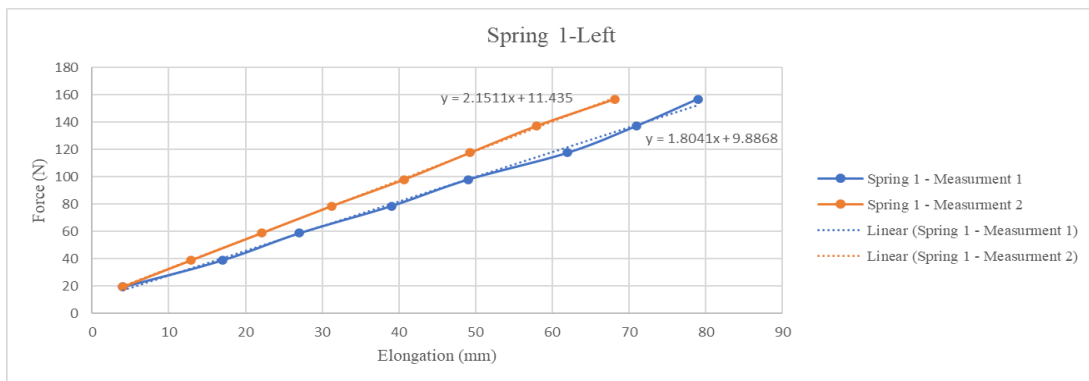


Figure 22: Left leg spring force (N) vs elongation (mm) graph

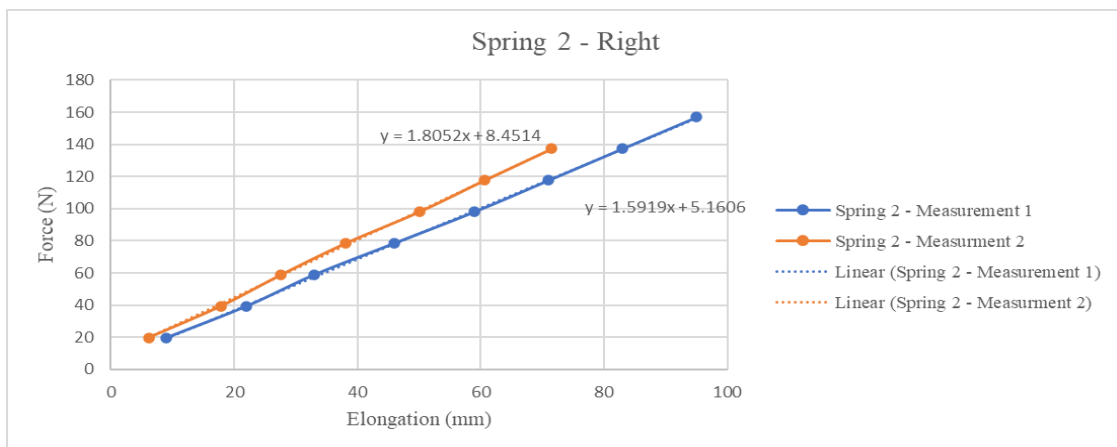


Figure 23: Right leg spring force (N) vs elongation (mm) graph

3.2 Test #2: Individual Link – Counter-Mass Balancing Test

For the side legs, the middle and distal links are balanced with a counter-mass. To verify that the produced counter-mass parts work as calculated in Chapter 2, some experiments are performed. The distal link has been hanged from the joint axis that connects the distal and middle link. The mass to be balanced for the distal link counter-mass are m_p and m_c as shown in Figure 3. The payload mass (m_p) is located 200 mm away from the joint axis, which exceeds the length of the distal link, but due to the design of the distal link by using moment equilibrium a new payload mass has been calculated where the payload mass could be located on the distal link for the balancing test. The experimental setup for the left distal link could be seen from Figure 24-25 and for right distal link from Figure 26-27.

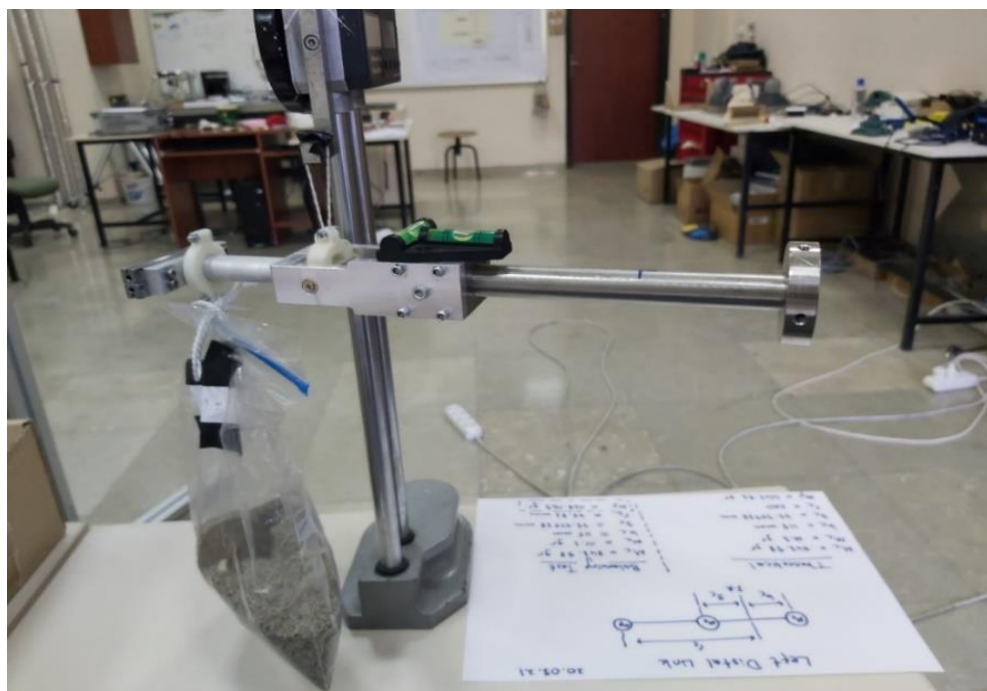


Figure 24: Balanced left distal link

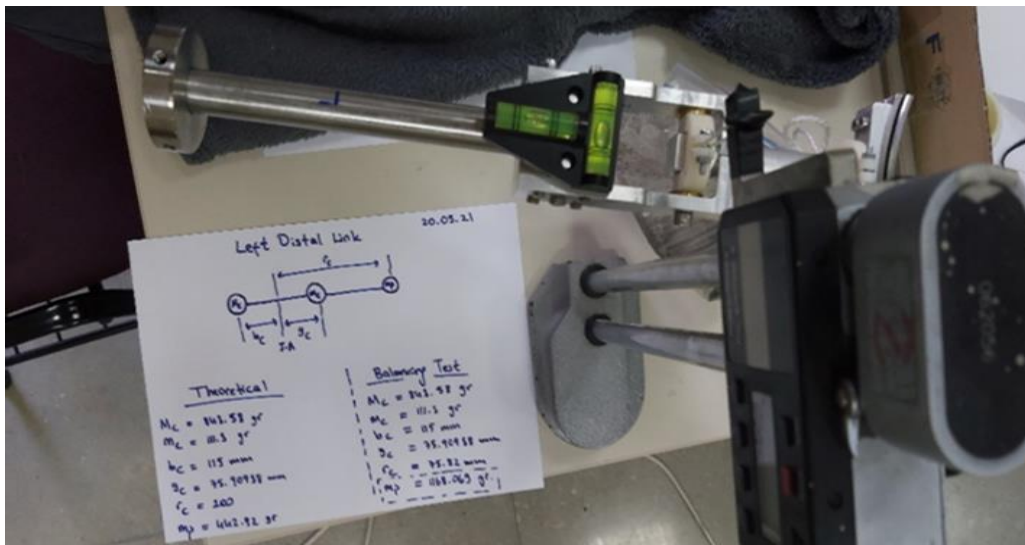


Figure 25: Balanced left distal link – 2



Figure 26: Balanced right distal link



Figure 27: Balanced right distal link – 2

To move the payload mass to the desired location on the distal link, an extra 3D printed part has been produced and its mass has been included in preparation of the payload mass. The balance state has been observed by placing a water level as near as possible to the joint axis and the location of the counter-mass cylinders have been adjusted and they are locked in the location where water gauge shows that the link is in balance with set screws.

Similar experiments are performed for the middle link for right and left legs. In these experiments, the counter-mass M_b should balance the desired mass which is the sum of M_c , m_p , m_c and m_b . The experimental setup for left middle link could be seen from Figure 28-29 and for the right middle link it could be seen from Figure 30-32.



Figure 28: Balanced left middle link

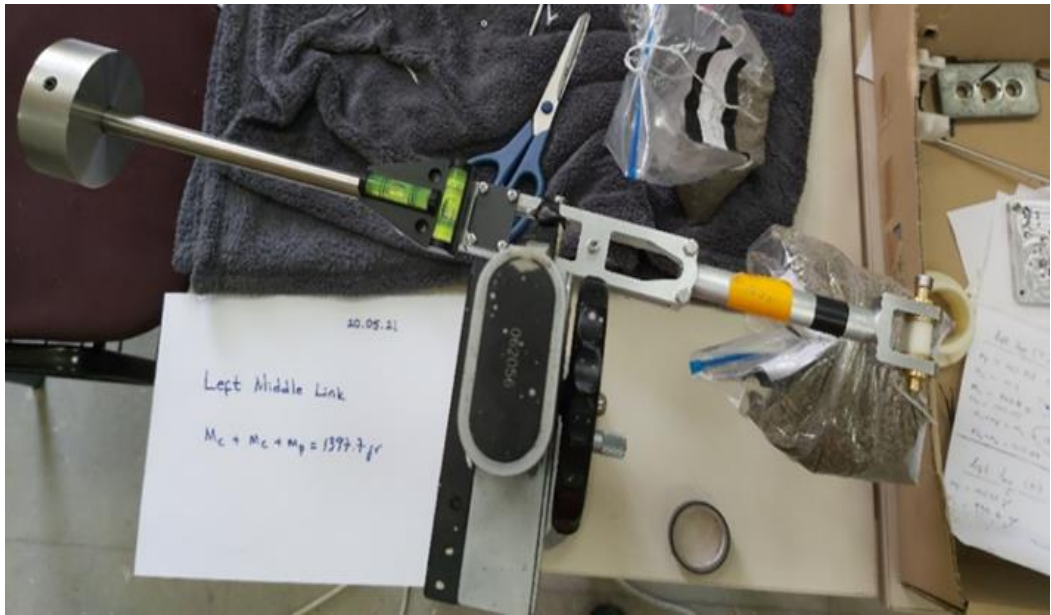


Figure 29: Balanced left middle link – 2



Figure 30: Balanced right middle link

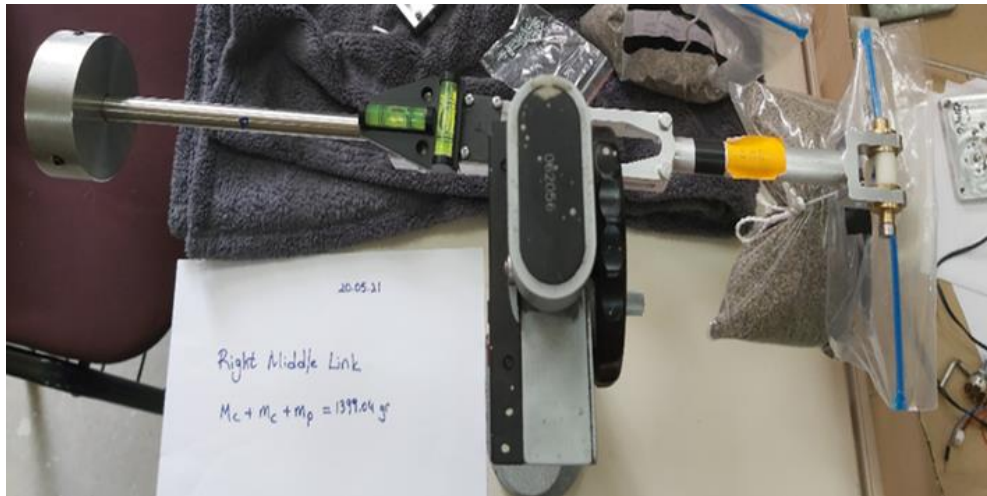


Figure 31: Balanced right middle link – 2

By reading water level from Figure 29 and Figure 31 it could be seen that the middle links for both legs are in balanced with their counter-mass. With these tests it has been shown that the links are able to stay in static balance with the desired payload and counter-mass and are ready to be assembled for the manipulator.

3.3 Test #3: Manipulator Assembled with Counter-Mass, Spring and Disabled Motors

The manipulator has three motors. Each leg has one motor where the middle motor is responsible for the heave motion, whereas the left and right motors generate motion to orient the end-effector. The transmission due to the gear reducer connected to the motor shafts generates friction. When the motors are enabled in the system the friction helps the system to stay in balance, therefore to observe that the system is in static balance the motors have been disconnected. All counter-mass components have been assembled with the distal and middle links for the left and right leg.

Because of lack of space on the base platform of the manipulator, an extra platform is positioned on top of the base platform in order to fix one of the ends of the.

The two springs are fixed at one end and are connected to a nylon coated steel wire to the free end. The two wires are connected to the proximal links of the side legs. The spring force acting on the proximal link theoretically could be anywhere on the line segment generated between a point on the link and A_0 (Figure 3). Connecting the wire directly to this line segment along the axis of the cylindrical link was not possible, so in order to generate the same behavior and to avoid the β angle explained in Chapter 2, a connection part has been designed as shown in Figure 30. This part is fixed to the link with the inner ring and the outer ring can rotate about an axis attached to the inner ring.

In Figure 32 the black line represents the wire and the red line represents the line segment generated between a point on the link and A_0 . As could be seen from Figure 32 when the wire surrounds the outer ring, its extension (shown with dashes) passes through the center of the inner ring which is on the red line. The steel wire is able to move around the outer ring within a groove and the outer ring is able to rotate around the inner ring.

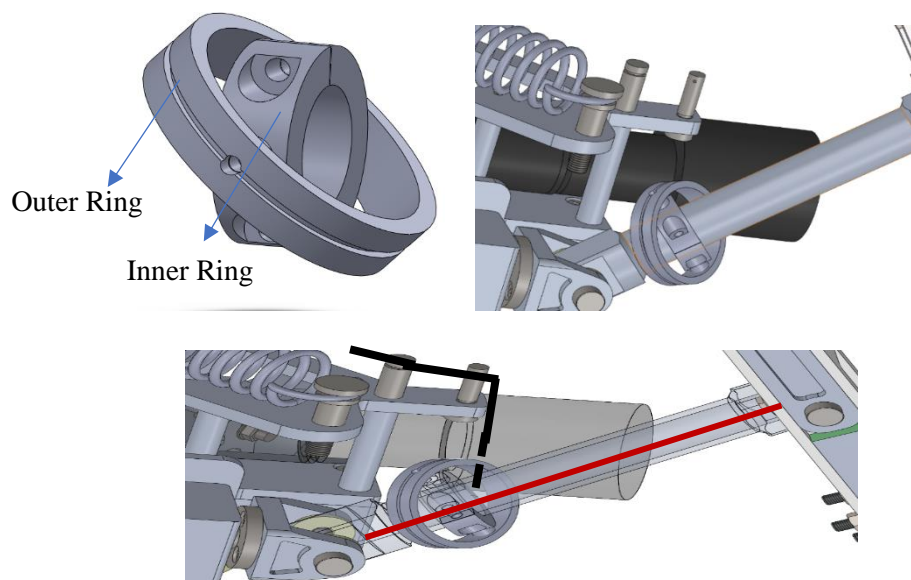


Figure 32: Wire connection to proximal link

To adjust the wire tension a part has been produced which is shown in Figure 33.

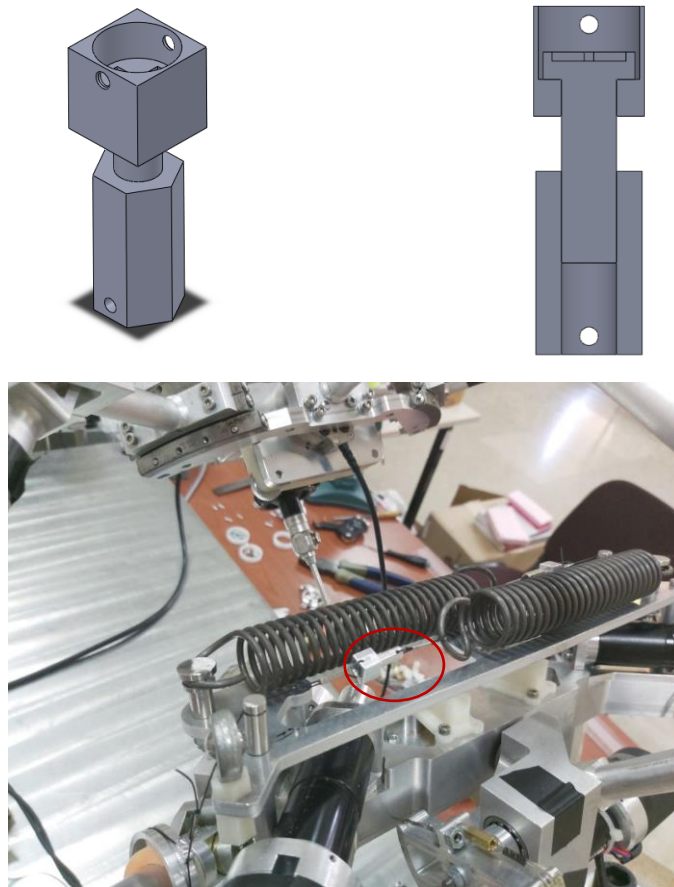


Figure 33: Wire tension adjustment

This equipment contains three parts which is a cubic part, a nut and a screw. The nut is connected to the spring's free end with a wire, whereas the cubic part is connected the outer ring on the proximal link with a wire. These two parts are connected to each other with a screw. Two sides of the system are in under tension because of the weight and the spring. When the screw is rotated while holding the cubic part, the nut generates a linear motion and the tension of the wire is adjusted. When the produced balancing components were assembled to the system according to the calculations made in Chapter 2, the system did not reach static balance because of the errors during the production of the parts and the uncalculated constraints of the system. When the system was left in a desired position the payload mass moved downwards, so to counter this effect additional 348 gr cylindrical steel blocks has been assembled to the middle link of each leg. The manufactured springs did not meet the design criteria so the position of the acting spring

force which is symbolized with “e” in Chapter 2 has been adjusted. This adjustment pushed the limit of the outer ring on the proximal link (Figure 33) which caused the wire to snap. To compensate this effect new springs which have a smaller spring coefficient has been manufactured. With the new springs the spring coefficient for the left leg has been changed from 1.8052 N/mm to 1.209 N/mm where “e_L” (e_L: e value for left leg) has changed from 26.13 mm to 39 mm, the spring coefficient for the right leg has been changed from 1.5919 N/mm to 1.137 N/mm where “e_R” (e_R: e value for left leg) has changed from 29.66 mm to 41.53 mm. When the “e” value increased for both of the legs the outer ring on the proximal link has been able to work without any difficulties.

After the adjustments on the counter-mass positions and the wire tension the system has achieved static balance which could be seen in Figure 34. Positioning the manipulator in different poses and observing the balance this test has been completed.

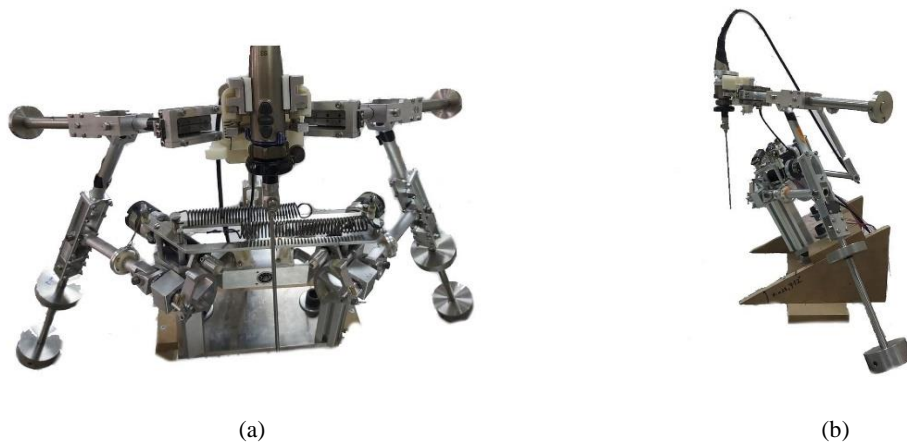


Figure 34: Balanced manipulator with motors disabled (a) front view, (b) side view

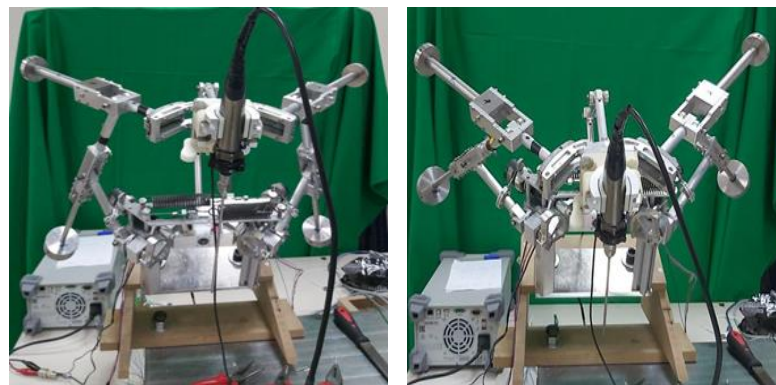
Due to eliminate some of the mechanical constraints balancing components has been adjusted and these changes are explained in Test #4. With the adjustments the workspace of the mechanism has been tested. The endoscope has been moved by hand without the motors and has been tried to be positioned at its border regions for x-axis, y-axis and z-axis. From Table 11 the positions of the endoscope could be seen.

Table 11: Position data from balanced manipulator with disabled motors

Position #	Endoscope Position (manually)		
	d (mm)	ϕ ($^{\circ}$)	ψ ($^{\circ}$)
1	250	-1.708	3.408
2	161.57	-3.381	-11.245
3	152.4	-19.097	-6.107
4	178.2	0.974	-11.135
5	137.57	-3.987	-14.698
6	226.95	-2.285	7.26

Table 12: Balanced manipulator with disabled motors workspace

Δd	$\Delta\phi$ ($^{\circ}$)	ψ ($^{\circ}$)
112.43	19.974	18.106



(a)

(b)

Figure 35: Balanced manipulator at (a) position #1 and (b) position #2



(a)

(b)

Figure 36: Balanced manipulator at (a) position #3 and (b) position #4

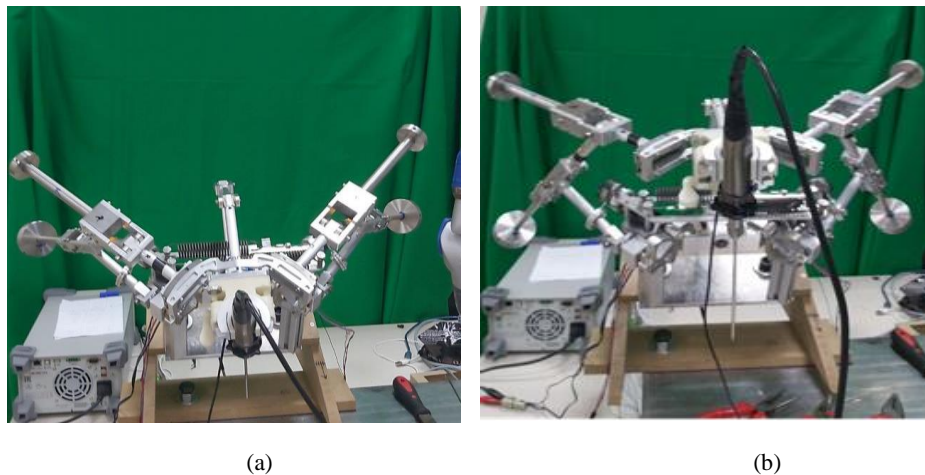


Figure 37: Balanced manipulator at (a) position #5 and (b) position #6

Because the end effector was manually moved when the endoscope was tried to positioned at one of its axis border regions the motion on the other two axis could not be blocked. From Table 11 the border regions for the motion around x-, y- axis and motion on the z- axis has been measured by using a measurement device, FARO, and has been shown in Table 11. The reason that the manipulator could not reach its border regions for the positive rotations around the y- axis is because of when the manipulator is driven from the end effector it required more torque than the manual input to position the endoscope. The endoscope could have been positively rotated around the x-axis more but because of the endoscope was wanted to move upward when the endoscope was released and the spring tension adjustments were done respect to this requirement, the left spring have obstructed the positive rotation around x-axis. The border regions that the manipulator could reach has been shown in Table 12.

3.4 Test #4: Parallel Manipulator Assembled with Counter-Mass, Spring and Running Motors

Before starting Test #4 to improve the manipulator back drivability, bearings have been placed on the pins where the wire coming from the free end of the springs passes on (shown in Figure 38 within the red circle).



Figure 38: Bearing added on the pin

Beforehand the wire was passing on the steel pin which made of the same material as the wire. The force on the pin, the friction between the same materials and the angle between the pin and the spherical joint caused stick-slip behavior. With this new adjustment the friction caused by the same material condition has been considerably reduced and a smoother motion for the manipulator has been obtained. Since friction was supporting the balancing, with the elimination of some these friction forces, new adjustments had to be made to the system.

Due to the decrease in friction and the increase in the force required to balance the system, the springs in the system became insufficient and the balance of the system was disturbed. To solve this problem the previous springs have been reinserted into the system because they had a higher spring coefficient where the left spring coefficient is $k_L = 1.8052 \text{ N/mm}$ and the right spring coefficient is $k_R = 1.5919 \text{ N/mm}$. With this adjustment, the cylinder blocks added as extra counter masses to middle links of the side legs are no longer needed. The position of where the spring force is acting on the proximal link has also been changed to ease the motion of the wire. The 3D printed inner ring shown in Figure 32 has been replaced by an aluminum version for more durability. By changing the position of the cylindrical block on the middle link extension link and the tension of the wire that is connected to the free end of the spring static balance has been achieved without the motors are enabled. The changes are shown in Table 13.

Table 13: Countermass Positions

e _L (mm)	48.85
e _R (mm)	44.15
a: Middle Link CM position _L (mm)	3.42
a: Middle Link CM position _R (mm)	11.27
a: Distal Link CM position _L (mm)	1.77
a: Distal Link CM position _R (mm)	1.2
Left proximal link wire length _L (mm)	147.5
Right proximal link wire length _R (mm)	182.5
k _R : Right spring coefficient (N/mm)	1.8052
k _L : Left spring coefficient (N/mm)	1.5919

Here, a is the distance that the cylindrical blocks should be positioned with respect to the edge of the cylindrical parts that they are positioned on, which is shown in Figure 39.

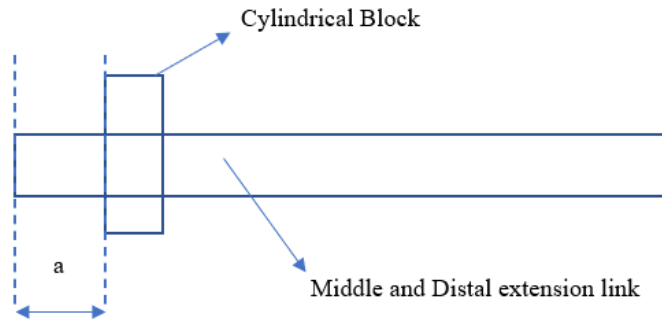


Figure 39: Cylindrical block position for middle and distal counter masses

With these adjustments, the tests for the case where the balancing components are assembled and motors are enabled are initiated. In these tests the balancing components are attached to the manipulator and the motors are enabled, to see the torque effects on the motors when they have to stay in a certain position and when there is motion. There are three individual conditions that have been changed. While one of the conditions is changing through its domain the other conditions has been tried to kept at their current positions. The rotation around the x-axis has been examined between -15° and 15° ,

rotation around y axis has been examined between -20° and 20° , and the motion on z axis has been examined between 150 mm and 250 mm.

The position data of the joints has been measured by using encoders. Then by using direct kinematic equations the position of the endoscope is calculated. The torque on the actuators is calculated as follows:

1. To drive the motors an ESCON 36/2 motor driver has been used and from the analog volt output the filtered real current values has been measured.
2. The analog output gives values between -4 V and $+4$ V. By using the computational program for the driver, the current that the motor is using has been mapped to the voltage values where 0 V gives 0 A and 4 V gives 2 A.
3. Using an LabJack brand data acquisition card the voltage values has been measured.
4. After mapping measured volt value to the current data, the torque value of the motor is obtained by multiplying the torque constant value found in the datasheet of the motor that has been used with the current value that has been obtained.
5. The torque value obtained is multiplied by the gear ratio and the torque values applied to the manipulator has been obtained.

To calculate the torque on the motors from the measured current:

$$T_i = \epsilon n K_T I_i \quad (3.1)$$

- Gear efficiency (ϵ) = %70
- Gear ratio (n) = 905
- Torque constant (K_T) = $11.5 * 10^{-3} \frac{Nm}{A}$
- Applied torque (T_i), $i: 1, 2, 3$
- Current (I_i), $i: 1, 2, 3$.

By using Equation 3.1, T_1 , T_2 and T_3 torque values are calculated as the left, right and middle motors, respectively.

In these tests the manipulator has been brought to the desired position and while the actuators are trying to hold the manipulator in the desired position the torque values generated by the actuators are measured. Seven different cases are investigated in these tests where the manipulator is brought to its border regions for each type of motion (yaw, pitch, heave) and the motors are locked at that position. During the motion where d decreases from 250 mm to 150 mm (insertion motion) there is no need of large rotations around the x - and y -axes during the operation. When the endoscope is positioned near the surgical area, rotations around x - and y -axes are generated where the amount of insertion of telescope of the endoscope should be about $d = 150$ mm.

The position data from the encoders are compared with measurements with the FARO device. For all seven positions the position of the endoscope, the angles between each link and the angles between the planes of each link has been measured. From Table 14 the position data for the balanced manipulator from the encoder and the position data from FARO could be seen. From Table 14 it could be seen that the position data of the endoscope from the encoder is different from the data collected with FARO. This difference is caused because when the actuator starts to work, the wire between the capstan and the shaft that is connected to the actuator slips and the wire tension gets loose. Also, the joint clearance and link deformations (Tables 15-16) effect the position data collected by the encoders.

Table 14: Balanced manipulator position data

	Balanced Manipulator Position Data					
	Endoscope Position (Encoder)			Endoscope Position (FARO)		
Position #	d	ϕ ($^{\circ}$)	ψ ($^{\circ}$)	d	ϕ ($^{\circ}$)	ψ ($^{\circ}$)
1	250	0	0	238.02	0.973	0.421
2	200	0	0	203.51	0	2.165
3	150	0	0	149.68	0.895	0.203
4	150	-15	0	168.96	-11.743	1.755
5	150	5	0	160.17	0.194	0.513
6	150	0	-20	136.11	0.426	-18.584
7	150	0	2	171.27	1.612	4.495

Table 15: Balanced manipulator joint clearance

Position #	Joint Clearance								
	Left Leg			Middle Leg			Right Leg		
	$\Delta\varepsilon$	$\Delta\rho$	$\Delta\tau$	$\Delta\varepsilon$	$\Delta\rho$	$\Delta\tau$	$\Delta\varepsilon$	$\Delta\rho$	$\Delta\tau$
1	2.93	-0.39	-1.09	4.5	1.57	0.06	1.95	0.55	-2.42
2	0.11	0.39	0.65	-2.6	4.22	-1.52	-3.49	4.21	-0.55
3	2.15	0.32	0.54	-0.74	2.31	-1.45	-4.58	4.63	-2.42
4	-2.23	2.37	-1.37	-0.22	1.94	-1.09	-2.76	-0.03	0.04
5	-5.03	5.25	4.5	-2.24	2.76	-0.92	1.69	0.47	-1.09
6	0.78	0.2	-0.98	3.35	-1.88	-0.54	4.38	-2.62	-1.38
7	1.7	0.59	0.29	-0.96	2.69	-0.35	-2.72	3.03	0.72

In Table 15 the joint clearance has been calculated by extracting the angle data calculated from MATLAB simulation from the angle data that has been collected with FARO. The angle between the base platform and the proximal link is denoted with ε , the angle between the proximal link and the middle link is denoted with ρ and the angle between the middle link and distal link is denoted with τ which is shown in Figure 40.

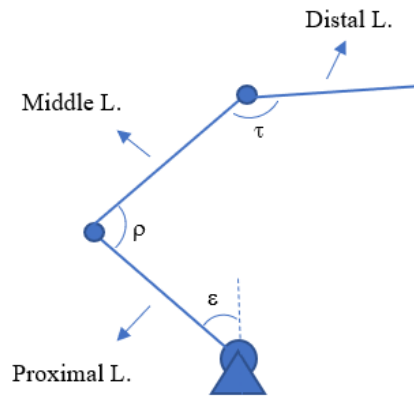


Figure 40: Illustration of the leg for the parallel manipulator

Theoretically, all three links of each limb should be coplanar, but in practice these links do not remain coplanar due to torsional deformations. The angle between the proximal link plane and middle link plane has been denoted with P-M plane angle and

the angle between the middle link plane and distal link plane has been denoted with M-D plane angle in Table 16.

Table 16: Plane angles measured with FARO for the balanced manipulator

Position #	Balanced Manipulator Plane Angles (all values in °)					
	Left Leg		Middle Leg		Right Leg	
	P-M Plane Angle	M-D Plane Angle	P-M Plane Angle	M-D Plane Angle	P-M Plane Angle	M-D Plane Angle
1	1.04	1.63	3.95	0.85	3.4	4.08
2	0.3	0.55	0.18	2.55	2.8	5.73
3	0.8	3	4.13	1.24	0.69	1.24
4	1.55	0.39	0.88	1.52	1.77	0.46
5	1.36	0.69	0.52	0.71	2.02	1.84
6	1.12	1.88	0.46	0.1	0.73	0.3
7	1.01	1.05	0.8	1.36	0.79	0.87

At position #5 the endoscope has been driven to the position where $d = 150\text{mm}, \phi = 5^\circ, \psi = 0^\circ$ and at position #7 the endoscope has been driven to the position where $d = 150\text{mm}, \phi = 0^\circ, \psi = 2^\circ$ (Table 14) and the required current for the motors to keep the endoscope for the desired position has been measured. The reason that the rotation around x-axis at position #5 is $\phi = 5^\circ$ (not 15°) and around y-axis at position #7 is $\psi = 2^\circ$ (not $\psi = 20^\circ$) is that when the endoscope is positioned at $d = 150, \phi = 0^\circ, \psi = 0^\circ$ and is tried to rotate around x-axis by 15° or by 20° around the y-axis, the part for the wire tension adjustment for the left spring collides with the pin.

For the balanced manipulator to stay in the desired position the required torque from each actuator has been shown in Table 17 and illustrated in Figure 41.

Table 17: Balanced manipulator torque results for each actuator

Balanced Torque Results			
Position #	T_1 (N·m)	T_2 (N·m)	T_3 (N·m)
1	0.725	1.795	2.8
2	2.1	0.02	1.4
3	0.25	1.49	0.55
4	1.4	0.4	2.9
5	9	1.5	1.25
6	2.3	0.03	0.1
7	4.5	0.015	4.95

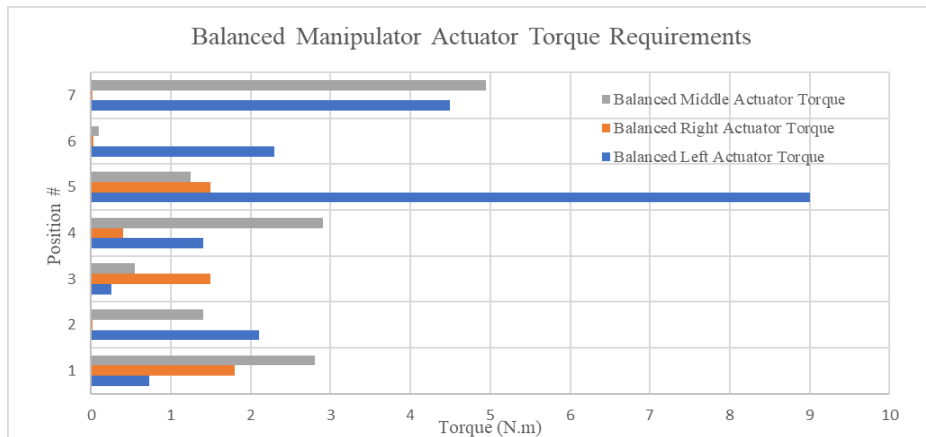


Figure 41: Balanced manipulator torque results for each position

To be able to compare these results with the unbalanced case, the balancing components are disassembled and the same tests are repeated. Due to the same reason during the balanced tests the position data collected by the encoders for the unbalanced manipulator is different from the measurements collected with FARO which could be seen from Table 18. Due to the inconsistency of the data collected from the encoders, the endoscope could not be brought to the same positions as the endoscope was in the balanced tests. The encoder data at the desired positions are the same as in the balanced tests, but the measurements from FARO are different (Table 18).

Table 18: Unbalanced manipulator position data

Position #	Unbalanced Manipulator Position Data					
	Endoscope (Encoder)			Endoscope (FARO)		
	d	ϕ (°)	ψ (°)	d	ϕ (°)	ψ (°)
1	250	0	0	214.76	0.276	-3.469
2	200	0	0	173.38	0.361	-2.051
3	150	0	0	129.61	0.74	2.818
4	150	-15	0	127	-16.306	-0.934
5	150	5	0	131.39	1.775	-3.491
6	150	0	-20	120.47	0.88	-19.767
7	150	0	2	134.6	2.365	0.694
8	150	15	0	139	15.139	1.595
9	150	0	20	154	0.309	21.213

For the unbalanced manipulator to stay in the desired positions shown in Table 16 the required torque from each actuator has been shown in Table 19 and illustrated in Figure 42.

Table 19: Unbalanced manipulator torque results for each actuator

Unbalanced Torque Results			
Position #	T ₁ (N·m)	T ₂ (N·m)	T ₃ (N·m)
1	4.5	1.6	2.97
2	3.1	3.26	1.7
3	0.9	2.9	0.9
4	1.45	2.5	2.1
5	0.44	1.4	0.7
6	4.15	2.7	1
7	1.4	3.27	1.54

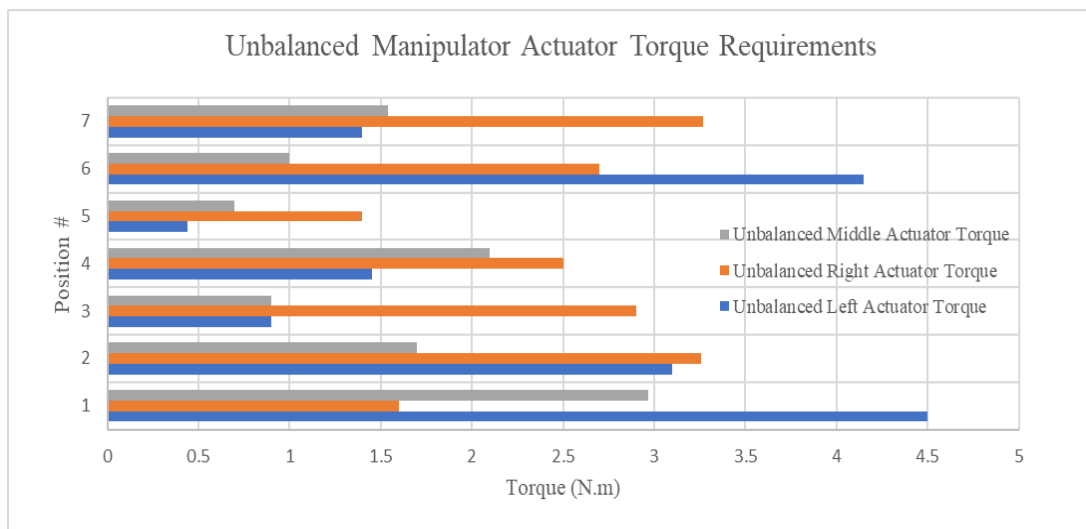


Figure 42: Unbalanced manipulator torque results for each position

CHAPTER 4

CONCLUSION

In this study a 2URRR-URR parallel manipulator has been statically balanced by using a hybrid spring and counter-mass balancing solution. Theoretically each of the three legs could be balanced, but because of the workspace with the applied solution, middle leg counter-masses would collide with the passive serial arm, therefore the payload mass has been distributed to the side legs. By adding counter-masses, distributed payload mass, distal and middle link masses have been relocated to the proximal link by using moment equilibrium where the static balancing problem has been reduced to balancing an inverted pendulum. With a moment equilibrium between the total leg mass and the applied spring force, the required spring coefficient has been calculated.

By analyzing the possibilities for the counter-masses and corresponding springs the torque effects on the motors have been simulated. From the simulation results it is seen that even though the counter-mass values and their position change, the motor torque values remain the same, which verifies that the static balancing has been successfully implemented. Due to this consistency the design specifications of these additional balancing parts have been selected to have the lightest weighted design. With the additional balancing parts, the systems total mass has been 10 kg which is within the desired limits. With balancing, the RMS torque on the motors has decreased from 3.08 N·m to 0.20 N·m which corresponds to a %93.5 decrease according to the simulation results.

There was not much space on the manipulator links or on the platforms to work on the manipulator and this effected the design and production of the balancing parts. With the first manufactured springs, there were several constructional problems such as the rotation limits of the outer ring (Figure 32) on the proximal link being insufficient. To relief the outer ring, new springs with lower spring coefficients have been manufactured. With this adjustment the position of the acting spring force on the proximal link has been modified and the problem has been solved. When the balanced manipulator motion is given by changing the position of the endoscope group and the motors are disabled the

motion is not fully smooth because of the wire tied to the free end of the spring passes two different pins which has the same material as the wire connected to the springs generated friction and restricted the movement of the spring. Even though the manipulator was in balance to lower the friction and ease the motion bearings has been placed on the pins. With this adjustment the friction between the wire connected to the springs and the pins has been minimized. Minimizing the friction in the balancing components disturbed the balance of the manipulator. The friction was working in a way of improving the balance with the minimization of the friction the springs has come insufficient. Due to this change the first springs where $k_L = 1.8052$ N/mm, $k_R = 1.5919$ N/mm has been reassembled to the system and the rearrangements for the balancing components has been done for the motors disabled case.

In Test #4 the required torque values from the actuators for the balanced and unbalanced manipulator has been calculated from the data collected. Due to mechanical constraints, the endoscope could not reach its boundary position for the positive rotations around the x- and y-axes. To check the position data, measurements are taken from the end-effector using the FARO device. From the results it has been seen that the encoder position data and the position data collected by FARO do not match due to joint clearances and flexibility of the links. Hence, the unbalanced manipulator endoscope could not be brought to the same positions as the balanced manipulator endoscope. The comparison between the balanced and unbalanced required torque values has been done from the encoder position data.

From the torque results for balanced case and unbalanced case when there is no rotation around the x- and y- axes and only motion along the z-axis where the motion is in the direction from position #1 to position #3 the required torque for the actuators has decreased. From the results it could be seen that the balancing components has decreased the required torque values.

When the manipulator is in position #4 where $d = 150$ mm, $\phi = -15^\circ$, $\psi = 0^\circ$ the negative rotation around the x-axis causes the right leg rotate more than the left leg which increases the spring elongation of the right spring more than the left spring. From the unbalanced torque results it could be seen that this effect the right actuator to provide more torque than the left actuator. For the balanced manipulator in position #4 due to the

balancing components the required torques has been decreased and also the required torque for the right actuator has been smaller than the left actuator.

When the manipulator has been brought to position #5, the positive rotation around the x-axis caused the left leg rotate more than right leg which has increased the left spring elongation more than the right spring. In this position for unbalanced case the same behavior at position #4 could not be examined. In this case the left actuator gave less torque than the right actuator. For the balanced case the spring tension adjustment is different for both of the springs where the left spring tension is tighter than the right spring and this affected the torque results. From the balanced torque results it could be seen that because of the tension adjustment for the left spring, the required torque value for the left actuator has peaked to its maximum value and the required torques in this position has exceeded the unbalanced torque results.

Where the manipulator could not be positioned at the same positions for the balanced and unbalanced cases, the closest matching data has been caught in position #6. In this specified position for the unbalanced case the highest torque value provided by the actuators is for the left actuator. With the balancing components assembled to the system the required torque for the left actuator has been decreased nearly 50% and the torque requirements for the right and middle actuator have nearly come to 0 N·m.

From the results the balancing components has made an effect on the required torques to stay in the specified positions. Generally, the required torques for the balanced manipulator are smaller than the unbalanced actuator torque requirements due to constructional constraints, but due to joint clearance and spring tension adjustments this behavior changes according to the position of the manipulator.

To have more comparable data, the joint clearances should be reduced. The tension adjustment for the left spring could be redone. With these adjustments the torque results would also improve.

To have a better balancing solution the base platform of the manipulator should have more space where the wire is connected to the free end of the spring would be able to connect to the proximal link by passing just one point. The actuator system for the manipulator contains the motor, gears and a capstan the reduction ratio of the actuation system is 1/905. Even though there is a high reduction ratio, the manipulator was unable to move due to the weight of the system. With statically balancing the system, the required

torque for the actuation system has been reduced. To improve the back drivability of the manipulator the gear system could be changed with a transmission system that has a lower gear ratio because of the decreased required torque for the actuation system.

Finally, it is demonstrated that the manipulator is balanced at different configurations within the end-effector workspace, where generally the required torque for the actuators on the balanced manipulator are smaller than the required torque for the actuators on the unbalanced manipulator. In the design process of the counter-masses one of the criteria was to not make any irreversible changes on the current links, which was a problem because there was not any available space on the linkages to connect the counter-masses. The links can be redesigned taking into account that there will be additional parts for balancing. Instead of just distributing the payload mass, the mass of the middle leg should have been distributed to the side legs as well to decrease the torque acting on the motors even more. For future works the distal and middle links could be designed in a better way to ease the assembly and design of the counter-masses, middle leg mass could be distributed to the side legs and new calculations and production of counter-masses could be made, base platform of the manipulator could be designed to have proper space for the springs. An extra degree of freedom could be added to the outer ring so that the wire would work better in all of the positions of the manipulator.

Throughout the thesis study, it has been seen that balancing a manipulator that has not been designed to be balanced is not practical. During the design process of the manipulator balancing should be included to avoid lack of space, link collisions and mechanical constraints. Using counter-mass to achieve static balance is more comfortable than using springs but with the added masses it increases the inertia of the system and the extensional links should be designed to avoid link collisions. For springs there should be a base for the springs and they do not work linearly, which changes the reaction of the spring due to its elongation which effects the balancing. In case of the hybrid solution of using springs and counter-masses to achieve static balance the balancing components design should be done during the design of the manipulator to smoothen the motion between the balancing components and the manipulator itself.

REFERENCES

Dede M.İ.C., Kiper G., Ayav T., Ateş G., Tatlıcıoğlu E., Özdemirel B., Maarroof O., Berker M., Işıkay İ., Hanalioğlu Ş. 2018. Cerrahin Anlık Yönlendirilebildiği Robot Yardımlı Endoskop Kontrol Sistemi Mimarisi – NeuRoboScope. Türkiye Robotbilim Konferansı (TORK 2018), İstanbul, 25-30

Ebert-Uphoff I., Gosselin C. M., Laliberté T. 2000, Static Balancing of Spatial Parallel Platform Mechanisms – Revisited, *Journal of Mechanical Design*, 122, 43-51

Herder J. L. 2001. Energy-Free Systems: Theory, Conception, and Design of Statically Balanced Spring Mechanisms. PhD-thesis, Delft University of Technology

Jean M., Gosselin C. M. (1996), Static Balancing of Planar Parallel Manipulators, In: Proc. IEEE International Conference on Robotics and Automation, Minneapolis, Minnesota, 3732-3737

Kilit Ö., İyim E. 2015. Düzlemsel Çubuk Mekanizmalarında Kam-Yay Yöntemi ile Ağırlık Dengelenmesi, Uluslararası Katılımlı 17. Makina Teorisi Sempozyumu Bildiri Kitabı, Makina Teorisi Derneği, Ankara, 536-541

Martini A., Troncossi M. Carricato M., Rivola A. 2015. Static Balancing of a Parallel Kinematics Machine with Linear-Delta Architecture: Theory, Design and Numerical investigation, *Mechanism and Machine Theory*, 90, 128-141

Martini A., Troncossi M., Rivola A. 2019. Algorithm for the Static Balancing of Serial and Parallel Mechanisms Combining Counterweights and Springs: Generation, Assessment and Ranking of Effective Design Variants, *Mechanism and Machine Theory*, 137, 336-354

Omar W Maroof, Saad Zaghlul Saeed and Mehmet İsmet Can Dede .2021. Partial Gravity Compensation of Surgical Robot, International Journal of Advanced Robotic Systems, 1-15

Russo A., Sinatra R., Xi F. 2005. Static Balancing of Parallel Robots, Mechanism and Machine Theory, 40, 191-202

Van Dorsser W. D., Barents R., Wisse B. M., Schenk M., Herder J. L. 2008. Energy-Free Adjustment of Gravity Equilibrators by Adjusting the Spring Stiffness, IMechE Part C: J. Mechanical Engineering Science, 222(9), 1839-1846

Wang J., Kong X. 2019. A Geometric Approach to the Static Balancing of Mechanisms Constructed Using Spherical Kinematic Chain Units, Mechanism and Machine Theory, 140, 305-320

Yaşır A., Kiper G., Dede M. İ. C., Van der Wijk V. 2019. Static Force Balancing of a 2R1T Parallel Manipulator with Remote Center of Motion. In: Uhl T. (ed). IFToMM WC 2019: Advances in Mechanism and Machine Science, Springer, Cham, 3219-3226